2009 Project Update

Fiber Optic Groundwater and Fisheries Study
(WMI Task 5.6)

Prepared by Bob Bower, Senior Hydrologist
Walla Walla Basin Watershed Council
December 17, 2009

OWEB Grant # 208-8002

Project Overview

The Fiber Optic Groundwater and Fisheries Study is a collaboration of the Walla Walla Basin Watershed Council (WWBWC), Oregon State University (OSU), and US Fish and Wildlife Service (USFWS) to carry out the most rigorous validation of stream temperature models ever attempted in the Walla Walla River Basin. During the winter to spring 2009, the WWBWC, OSU and USFWS staff worked together to develop a 2009 field strategy for the project that would encapsulate both the fisheries and the groundwater-instream scientific questions being tested with this multidisciplinary project. Research questions were developed and exchanged amongst the partners. Data from the 2008 season was shared amongst the three research partners and a field plan for deployment and testing developed via conference calls and online meeting software.

For more information on the jointly-developed study plan please see the 2008 report submitted to OWEB. As outlined in the study plan, the objectives of this project are to: 1) Determine specific groundwater inflow locations along the Oregon and Washington study sections of the Walla Walla River; 2) Quantify groundwater inflow and temperature reduction locations in the study sections of the river and; 3) Cross reference groundwater inflow occurrence and quantities with fish species, life history, and habitat information.

Groundwater inflow locations were determined using temperature as the primary indicator since groundwater enters the stream system cooler than the river channel water. Fiber Optic Distributed Temperature Sensing (DTS)[1] technology allows for measurement of temperature to 0.01 deg C every meter along the river bed using standard communication fibers. Data can be obtained as often as every 1 minute along the entire cable, with the instrument capable of immediate wireless communication of these data via cell or satellite connections.

Groundwater and temperature reduction locations in the study reach were determined though a detailed survey of the physical stream features and shade. Seepage runs, or instantaneous flow measurements taken throughout the reach, were used to quantify the gain and loss of water to the system, and therefore quantify the groundwater inflow. This aspect of the project was also conducted by OSU and WWBWC.

[1] http://www.sensornet.co.uk/products-&-systems/sentinel-dts-product-range.cfm
http://cp.literature.agilent.com/litweb/pdf/5989-4500EN.pdf

Finally, groundwater inflow occurrence was cross-referenced with fish snorkel surveys taken by the USFWS along the fiber optics reach in the summer.

2009 Field Work

Field work on the Fiber Optic Groundwater and Fisheries study in 2009 continued to prove to be both productive and challenging. Whilst many of the issues that arouse in 2008 were fixed or improved upon (e.g. new thicker cable deployed and new DTS system purchased) there still remained in-situ challenges for the project. However, WWBWC and OSU staff learned how to make the project more efficient and effective over this field season, and the data collected was of better quality than that collected the previous season. The field activities and data collection are summarized below in accordance to the three major objectives of the project.

Objective 1: Determine specific groundwater inflow locations

In July 2009 roughly 6000 meters of fiber optic cable were deployed in the mainstem Walla Walla river from Mauer Lane downstream to the Bier farm, which is just south of the state line. Staff and students from WWBWC and OSU reeled the cable out and covered with rocks to keep it on the river bed along both banks of the river. The DTS computer logging the data was installed in a safe box at Mauer lane. A refrigerator was purchased and DTS placed inside in an attempt to cool the system during the hottest of summer days. Also the pump station where power is provided from John Mauer was rewired by a local electrical contractor to ensure undisrupted supply for the 2009 season.

The 2009 fiber optics cable was building specific for riverine deployments and did not need splicing or replacing during the entire field season. In addition to the continuous temperature from the fiber optics cable, temperature loggers were deployed along the cable length as a calibration-reference for the cable data. Also flow stations were also deployed to measure flow during the field season at key locations. Finally, the cable and all field equipment were retrieved in late November by WWBWC and OSU.

Objective 2: Quantify groundwater inflow and temperature reduction locations

Three additional and complementary research projects were performed in the fiber optic section of the river this summer to complement and help quantify objective 2. Firstly a LIDAR flight (**Attachment 1**) was flown by *Watershed Sciences* in order to provide extremely accurate gradient and elevation data for the project. The fiber optic cable was also surveyed with a *Trimble Survey Grade GPS* system to ensure good location information relative to the LIDAR flight and groundwater conditions. Also a electrical resistivity survey was performed by OSU and Rutger Universities in conjunction with the USGS. A scope of work was put together by the OSU team **(Attachment 2)** which highlights the benefits of this high resolution subsurface mapping technique to complement the fiber optic research.

OSU graduate students also installed in channel piezometer grids in three locations along the fiber optic cables length. These were installed as physical reference points to calibrate the fiber optic information (e.g. groundwater exchanges) against. As the Walla Walla River channel changed extensively from the previous season, another extensive survey and

documentation of the physical characteristics of the fiber optics reach was conducted throughout the summer in order to compare the continuous temperature data to the reach's geomorphological conditions. Specifically, it allowed us to assess correlations between channel morphology and hyporheic and groundwater temperature information. GPS coordinates of all gravel bars, pools, and suspected groundwater seeps were noted along with the cable meter number for reference the to the fiber optics temperature data. Other detailed notes and coordinates were taken on areas of beaver activity, sections where the cable was exposed to the air, and points of agricultural and irrigation inflows. Also a survey of effective shade along the reach was conducted using a solar pathfinder.

Objective 3: Cross reference groundwater and fisheries data

Using the field strategy discussed during the winter of 2008-9 the USFWS assisted the OSU team in determining some key locations on which to focus the establishment of the aforementioned piezometers GRIDS. They also conducted three fisheries and habitat surveys throughout the field season.

2009 Analysis Work
Data analysis for the Fiber Optics and Fisheries Study and QA/QC started in December 2009 with the final report available in November 2010.

2009 Outreach Work
The WWBWC, USFWS and OSU presented this study at the Watershed Management Initiative Technical Review Team meeting to regional scientists on December 10, 2009

Future Work
2010 marks the final year of this project. This will be a non-field work year, focusing instead on pulling together all the information collected during the two field seasons into a concise and final project report and papers. Results from all of this information will be presented and provided in electronic and paper form to OWEB and all of the partners and interested parties on this project.

The final report for this project will be completed on November 30th, 2010.

Appendices I

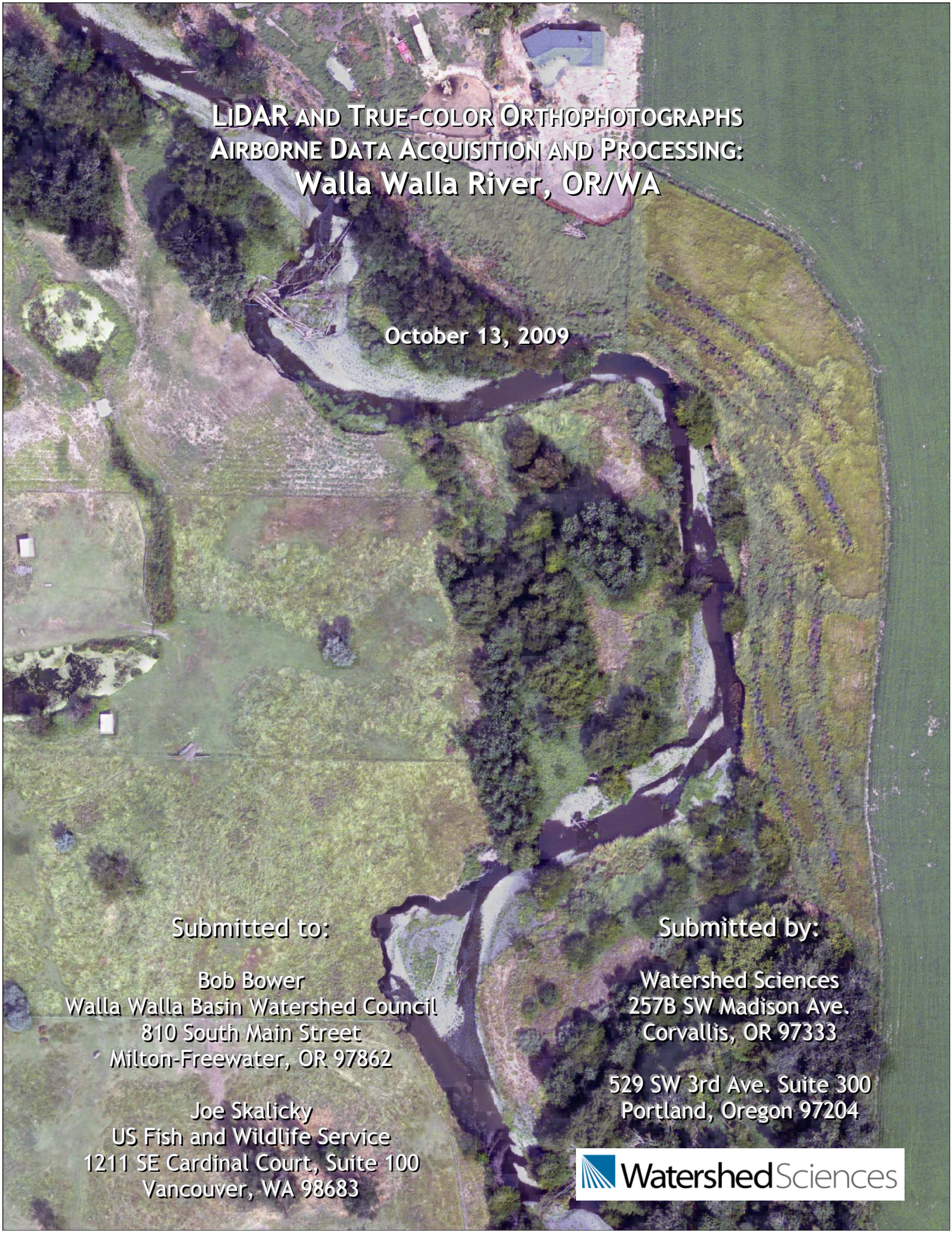

LiDAR and True-color Orthophotographs Airborne Data Acquisition and Processing:
Walla Walla River, OR/WA

October 13, 2009

Submitted to:

Bob Bower
Walla Walla Basin Watershed Council
810 South Main Street
Milton-Freewater, OR 97862

Joe Skalicky
US Fish and Wildlife Service
1211 SE Cardinal Court, Suite 100
Vancouver, WA 98683

Submitted by:

Watershed Sciences
257B SW Madison Ave.
Corvallis, OR 97333

529 SW 3rd Ave. Suite 300
Portland, Oregon 97204

Watershed Sciences

LiDAR and True-color Orthophotographs
Airborne Data Acquisition and Processing:
Walla Walla River, OR/WA

TABLE OF CONTENTS

1. Overview 4
2. Acquisition 5
   2.1 Airborne Survey – Instrumentation and Methods 5
   2.2 Ground Survey – Instrumentation and Methods 6
      2.2.1 Survey Control 6
      2.2.2 RTK Survey 6
3. Data Processing 8
   3.1 Applications and Work Flow Overview 8
   3.2 Aircraft Kinematic GPS and IMU Data 9
   3.3 Laser Point Processing 9
   3.4 Orthophotograph Processing 10
4. LiDAR Accuracy Assessment 10
   4.1 Laser Noise and Relative Accuracy 10
   4.2 Absolute Accuracy 11
5. Photo Accuracy Assessment 12
6. Study Area Results 13
   6.1 Data Summary 13
   6.2 LiDAR Point Density/Resolution 13
   6.3 LiDAR Relative Accuracy Calibration Results 16
   6.4 LiDAR Absolute Accuracy 16
   6.5 Orthophotograph Accuracy 18
   6.5 Projection/Datum and Units 20
7. Deliverables 20
8. Selected Images 21
9. Glossary 23
10. Citations 25
Appendix A 26

1. Overview

Watershed Sciences, Inc. (WS) collected Light Detection and Ranging (LiDAR) data and true-color orthophotographs on a 4 mile stretch of the Walla Walla River and its riparian area on August 17th, 2009. This report contains the LiDAR and true-color orthophotograph data and analysis. The total area delivered is 859 acres (**Figure 1**). The requested area was expanded to include a 100 m buffer to ensure complete coverage and adequate LiDAR point densities around survey area boundaries.

Figure 1. Walla Walla River study area.

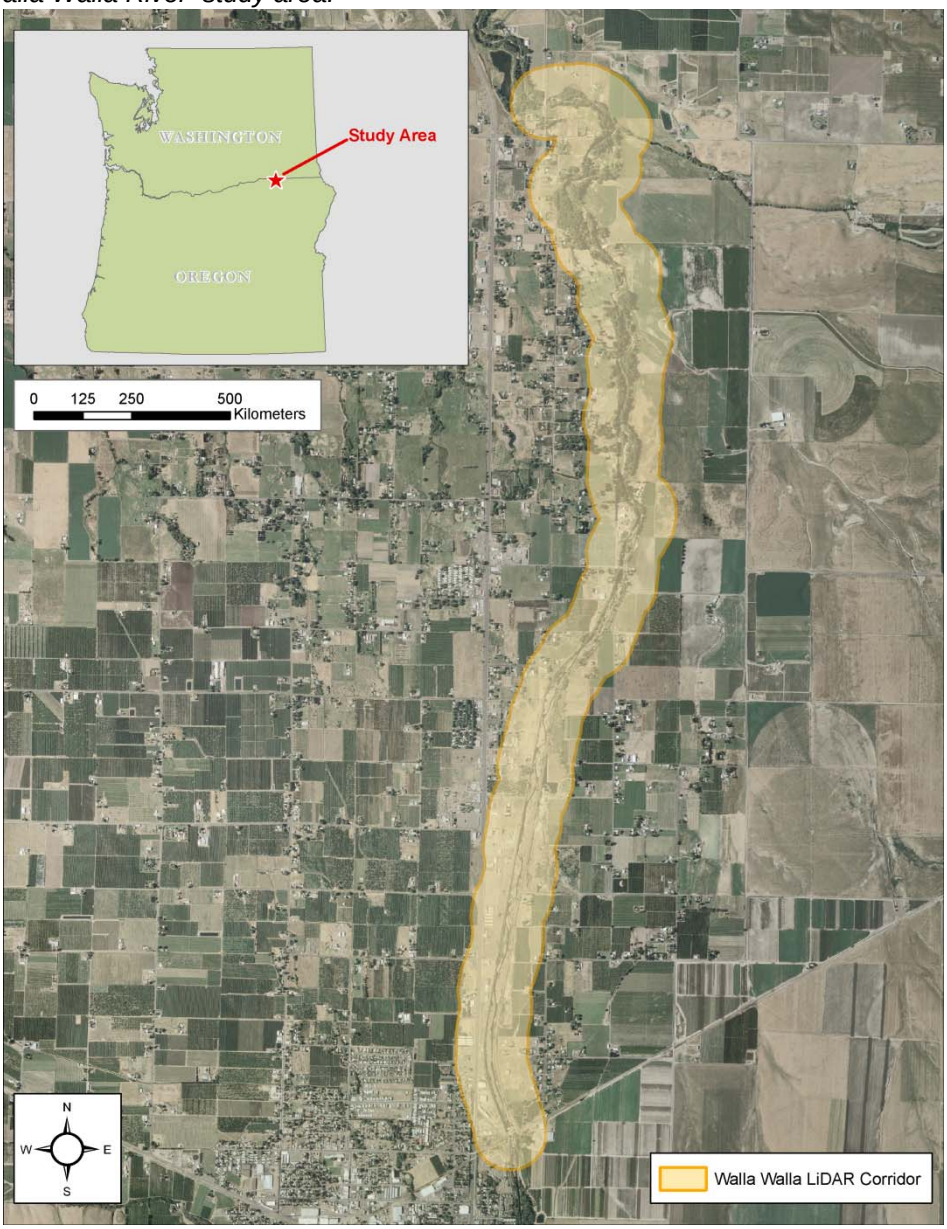

2. Acquisition

2.1 Airborne Survey – Instrumentation and Methods

The LiDAR survey used a Leica ALS50 Phase II laser system. For the Walla Walla River survey site, the sensor scan angle was ±15° from nadir[1] with a pulse rate designed to yield an average native density (number of pulses emitted by the laser system) of ≥ 8 points per square meter over terrestrial surfaces. All survey areas were surveyed with an opposing flight line side-lap of ≥50% (≥100% overlap) to reduce laser shadowing and increase surface laser painting. The Leica ALS50 Phase II system allows up to four range measurements (returns) per pulse, and all discernable laser returns were processed for the output dataset.

The aerial imagery was collected using a Leica RCD-105 39 megapixel digital camera. For the Walla Walla River survey site, images were collected in 3 spectral bands (red, green, blue) with 60% along track overlap and 30% sidelap between frames. The acquisition flight parameters were designed to yield native pixel resolution of ≤15cm.

The Cessna Caravan is a stable platform, ideal for flying slow and low for high density projects. The Leica ALS50 sensor head installed in the Caravan is shown on the left.

To accurately solve for laser point position (geographic coordinates x, y, z), the positional coordinates of the airborne sensor and the attitude of the aircraft were recorded continuously throughout the LiDAR and photo collection mission. Aircraft position was measured twice per second (2 Hz) by an onboard differential GPS unit. Aircraft attitude was measured 200 times per second (200 Hz) as pitch, roll and yaw (heading) from an onboard inertial measurement unit (IMU). To allow for post-processing correction and calibration, aircraft/sensor position and attitude data are indexed by GPS time.

[1] Nadir refers to the perpendicular vector to the ground directly below the aircraft. Nadir is commonly used to measure the angle from the vector and is referred to a "degrees from nadir".

2.2 Ground Survey – Instrumentation and Methods

The following ground survey data were collected to enable the geo-spatial correction of the aircraft positional coordinate data collected throughout the flight, and to allow for quality assurance checks on final LiDAR data products.

2.2.1 Survey Control

Simultaneous with the airborne data collection mission, multiple static (1 Hz recording frequency) ground surveys were conducted over monuments with known coordinates in the Walla Walla River survey area (**Table 1**). Indexed by time, these GPS data are used to correct the continuous onboard measurements of aircraft position recorded throughout the mission. Multiple sessions were processed over the same monument to confirm antenna height measurements and reported position accuracy. Controls were located within 13 nautical miles of the mission area.

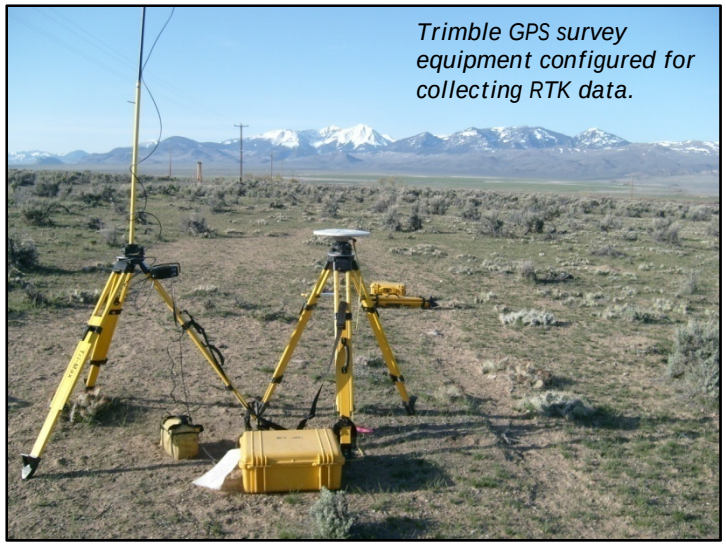

Trimble GPS survey equipment configured for collecting RTK data.

Table 1. Base Station Survey Control coordinates for the Walla Walla River survey area.

Base Station ID	Datum: NAD83 (CORS91)		GRS80
	Latitude	Longitude	Ellipsoid Z
WW_EG1	45° 58′ 10.80869″	118° 23′ 15.12315″	250.495
WW_EG2	45° 58′ 31.57305″	118° 22′ 18.10560″	241.664

2.2.2 RTK Survey

To enable assessment of LiDAR data accuracy, ground truth points were collected using GPS based real-time kinematic (RTK) surveying. For an RTK survey, the ground crew uses a roving unit to receive radio-relayed corrected positional coordinates for all ground points from a GPS base station set up over a survey control monument. Instrumentation includes multiple Trimble DGPS units (R8). RTK surveying allows for precise location measurements with an error (σ) of ≤ 1.5 cm (0.6 in). **Figure 2** below portrays a distribution of RTK point locations used for the survey areas.

Figure 2. RTK locations used for the Walla Walla River survey area (252 RTK points collected).

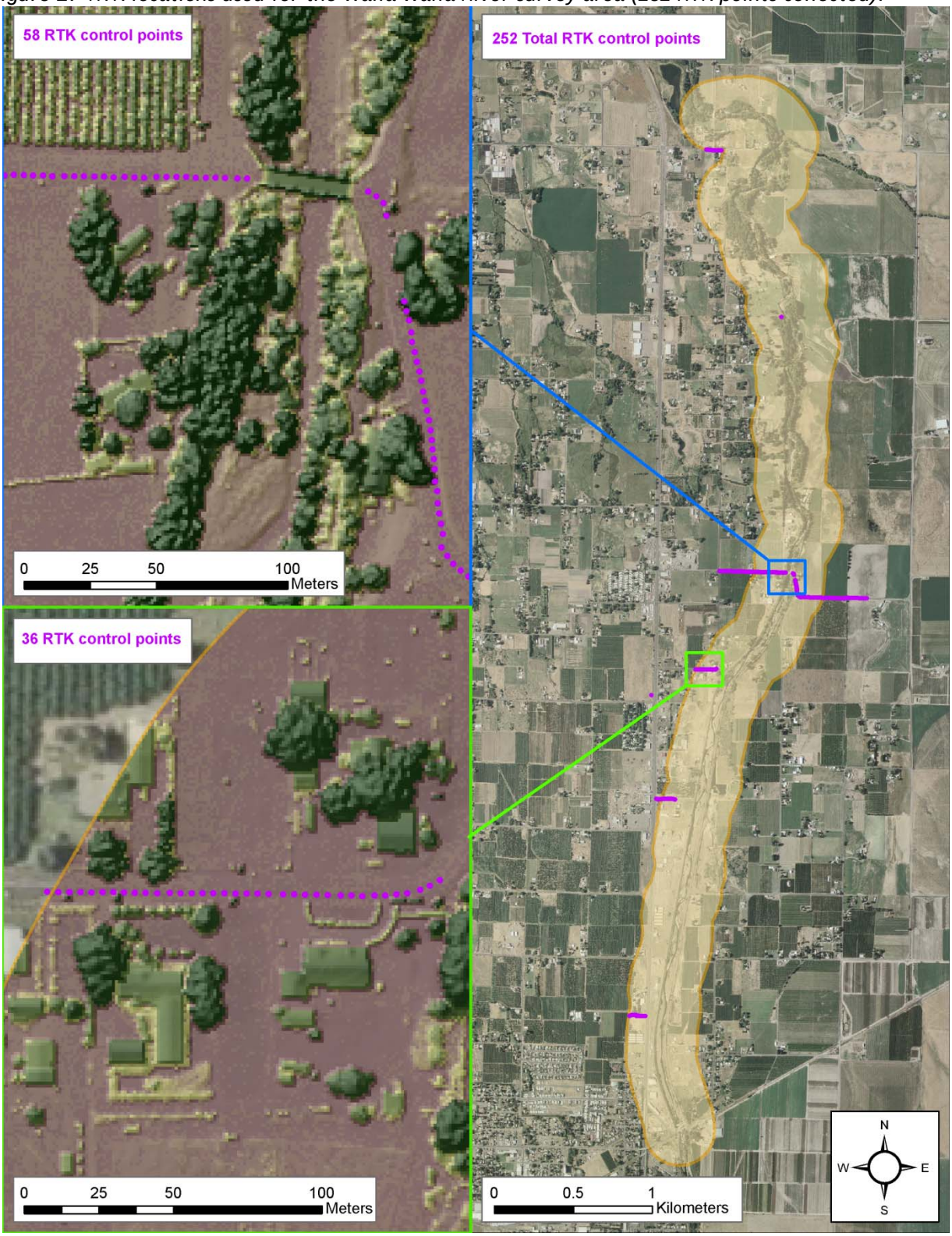

3. Data Processing

3.1 Applications and Work Flow Overview

1. Resolved kinematic corrections for aircraft position data using kinematic aircraft GPS and static ground GPS data.

   Software: Waypoint GPS v.8.10, Trimble Geomatics Office v.1.62
2. Developed a smoothed best estimate of trajectory (SBET) file that blends post-processed aircraft position with attitude data Sensor head position and attitude were calculated throughout the survey. The SBET data were used extensively for laser point processing.

   Software: IPAS v.1.4
3. Calculated laser point position by associating SBET position to each laser point return time, scan angle, intensity, etc. Created raw laser point cloud data for the entire survey in *.las (ASPRS v1.1) format.

   Software: ALS Post Processing Software v.2.69
4. Imported raw laser points into manageable blocks (less than 500 MB) to perform manual relative accuracy calibration and filter for pits/birds. Ground points were then classified for individual flight lines (to be used for relative accuracy testing and calibration).

   Software: TerraScan v.9.001
5. Using ground classified points per each flight line, the relative accuracy was tested. Automated line-to-line calibrations were then performed for system attitude parameters (pitch, roll, heading), mirror flex (scale) and GPS/IMU drift. Calibrations were performed on ground classified points from paired flight lines. Every flight line was used for relative accuracy calibration.

   Software: TerraMatch v.9.001
6. Position and attitude data were imported. Resulting data were classified as ground and non-ground points. Statistical absolute accuracy was assessed via direct comparisons of ground classified points to ground RTK survey data. Data were then converted to orthometric elevations (NAVD88) by applying a Geoid03 correction. Ground models were created as a triangulated surface and exported as ArcInfo ASCII grids at a 1-meter pixel resolution.

   Software: TerraScan v.9.001, ArcMap v9.3, TerraModeler v.9.001
7. Converted raw images to tif format, calibrating raw image pixels for gain and exposure settings of each image.

   Software: Leica Calibration Post Processing v.1.0.4
8. Calculated photo position and orientation by associating the SBET position (Step 3) to each image capture time.

   Software: IPASCO v.1.3
9. Orthorectified calibrated tiffs utilizing photo orientation information (Step 8) and the LiDAR-derived ground surface (Step 6).

   Software: Leica Photogrammetry Suite v.9.2
10. To correct light imbalances between overlapping images, radiometric global tilting adjustments were applied to the rectified images.

    Software: OrthoVista v.4.2.
11. The color corrected images were then mosaicked together for the survey area and subset into tiles to make the file size more manageable.

    Software: OrthoVista v.4.2.

3.2 Aircraft Kinematic GPS and IMU Data

LiDAR survey datasets were referenced to the 1 Hz static ground GPS data collected over pre-surveyed monuments with known coordinates. While surveying, the aircraft collected 2 Hz kinematic GPS data, and the onboard inertial measurement unit (IMU) collected 200 Hz aircraft attitude data. Leica IPAS Suite was used to process the kinematic corrections for the aircraft. The static and kinematic GPS data were then post-processed after the survey to obtain an accurate GPS solution and aircraft positions. Waypoint was used to develop a trajectory file that includes corrected aircraft position and attitude information. The trajectory data for the entire flight survey session were incorporated into a final smoothed best estimated trajectory (SBET) file that contains accurate and continuous aircraft positions and attitudes.

3.3 Laser Point Processing

Laser point coordinates were computed using the Leica ALS Post Processor software based on independent data from the LiDAR system (pulse time, scan angle), and aircraft trajectory data (SBET). Laser point returns (first through fourth) were assigned an associated (x, y, z) coordinate along with unique intensity values (0-255). The data were output into large LAS v. 1.1 files; each point maintains the corresponding scan angle, return number (echo), intensity, and x, y, z (easting, northing, and elevation) information.

These initial laser point files were too large for subsequent processing. To facilitate laser point processing, bins (polygons) were created to divide the dataset into manageable sizes (< 500 MB). Flightlines and LiDAR data were then reviewed to ensure complete coverage of the survey area and positional accuracy of the laser points.

Laser point data were imported into processing bins in TerraScan, and manual calibration was performed to assess the system offsets for pitch, roll, heading and scale (mirror flex). Using a geometric relationship developed by Watershed Sciences, each of these offsets was resolved and corrected if necessary.

LiDAR points were then filtered for noise, pits (artificial low points) and birds (true birds as well as erroneously high points) by screening for absolute elevation limits, isolated points and height above ground. Each bin was then manually inspected for remaining pits and birds and spurious points were removed. In a bin containing approximately 7.5-9.0 million points, an average of 50-100 points are typically found to be artificially low or high. Common sources of non-terrestrial returns are clouds, birds, vapor, haze, decks, brush piles, etc.

Internal calibration was refined using TerraMatch. Points from overlapping lines were tested for internal consistency and final adjustments were made for system misalignments (i.e., pitch, roll, heading offsets and scale). Automated sensor attitude and scale corrections yielded 3-5 cm improvements in the relative accuracy. Once system misalignments were corrected, vertical GPS drift was then resolved and removed per flight line, yielding a slight improvement (<1 cm) in relative accuracy.

The TerraScan software suite is designed specifically for classifying near-ground points (Soininen, 2004). The processing sequence began by 'removing' all points that were not 'near' the earth based on geometric constraints used to evaluate multi-return points. The resulting bare earth (ground) model was visually inspected and additional ground point modeling was performed in site-specific areas to improve ground detail. This manual editing of grounds often occurs in areas with known ground modeling deficiencies, such as: bedrock outcrops, cliffs, deeply incised stream banks, and dense vegetation. In some cases, automated ground point classification erroneously included known vegetation (i.e., understory, low/dense shrubs, etc.). These points were manually reclassified as non-grounds. Ground surface rasters were developed from triangulated irregular networks (TINs) of ground points.

3.4 Orthophotograph Processing

Image radiometric values were calibrated to specific gain and exposure settings associated with each capture using Leica's Calibration Post Processing software. The calibrated images were saved in tiff format to be used as inputs for the rectification process.
Photo position and orientation was then calculated by assigning aircraft position and attitude information to each image by associating the time of image capture with trajectory file (SBET) in IPASCO. Photos were then orthorectified to the LiDAR derived ground surface using LPS. This typically results in <2 pixel relative accuracy between images. Relative accuracy can vary slightly with terrain but offsets greater than 2 pixels tend to manifest at the image edges which are typically removed in the mosaic process.

The rectified images were mosaicked together in a three step process using Orthovista. Firstly color correction was applied to each image using global tilting adjustments designed to homogenize overlapping regions. Secondly, discrepancies between images were minimized by an automated seam generation process. The most nadir portion of each image was selected and seams were drawn around landscape features. The requested tile delineation (1/16th USGS quads) was too large for the high-resolution orthophotos, therefore the orthophotos were re-delineated into a more manageable size (~2000 x 2000m) appropriate to the pixel resolution and requested spatial reference.

4. LiDAR Accuracy Assessment

Our LiDAR quality assurance process uses the data from the real-time kinematic (RTK) ground survey conducted in the survey area. In this project, a total of **252 RTK** GPS measurements were collected on hard surfaces distributed among multiple flight swaths. To assess absolute accuracy, we compared the location coordinates of these known RTK ground survey points to those calculated for the closest laser points.

4.1 Laser Noise and Relative Accuracy

Laser point absolute accuracy is largely a function of laser noise and relative accuracy. To minimize these contributions to absolute error, we first performed a number of noise filtering and calibration procedures prior to evaluating absolute accuracy.

Laser Noise
For any given target, laser noise is the breadth of the data cloud per laser return (i.e., last, first, etc.). Lower intensity surfaces (roads, rooftops, still/calm water) experience higher laser noise. The laser noise range for this survey was approximately 0.02 meters.

Relative Accuracy
Relative accuracy refers to the internal consistency of the data set - the ability to place a laser point in the same location over multiple flight lines, GPS conditions, and aircraft attitudes. Affected by system attitude offsets, scale, and GPS/IMU drift, internal consistency is measured as the divergence between points from different flight lines within an overlapping area. Divergence is most apparent when flight lines are opposing. When the LiDAR system is well calibrated, the line-to-line divergence is low (<10 cm). See Appendix A for further information on sources of error and operational measures that can be taken to improve relative accuracy.

Relative Accuracy Calibration Methodology

1. Manual System Calibration: Calibration procedures for each mission require solving geometric relationships that relate measured swath-to-swath deviations to misalignments of system attitude parameters. Corrected scale, pitch, roll and heading offsets were calculated and applied to resolve misalignments. The raw divergence between lines was computed after the manual calibration was completed and reported for each survey area.
2. Automated Attitude Calibration: All data were tested and calibrated using TerraMatch automated sampling routines. Ground points were classified for each individual flight line and used for line-to-line testing. System misalignment offsets (pitch, roll and heading) and scale were solved for each individual mission and applied to respective mission datasets. The data from each mission were then blended when imported together to form the entire area of interest.
3. Automated Z Calibration: Ground points per line were utilized to calculate the vertical divergence between lines caused by vertical GPS drift. Automated Z calibration was the final step employed for relative accuracy calibration.

4.2 Absolute Accuracy

The vertical accuracy of the LiDAR data is described as the mean and standard deviation (sigma ~ σ) of divergence of LiDAR point coordinates from RTK ground survey point coordinates. To provide a sense of the model predictive power of the dataset, the root mean square error (RMSE) for vertical accuracy is also provided. These statistics assume the error distributions for x, y, and z are normally distributed, thus we also consider the skew and kurtosis of distributions when evaluating error statistics.

Statements of statistical accuracy apply to fixed terrestrial surfaces only and may not be applied to areas of dense vegetation or steep terrain. To calibrate laser accuracy for the LiDAR dataset, 252 RTK points were collected on fixed, hard-packed road surfaces within the survey area.

5. Photo Accuracy Assessment

To assess spatial accuracy of the orthophotographs they are compared against control points identified from the LIDAR intensity images. The control points were collected and measured on surface features such as painted road-lines, and boulders in the stream beds. The accuracy of the final mosaic, expressed as root mean square error (RMSE), was calculated in relation to the LiDAR-derived control points. **Figure 3** displays the co-registration between orthorectified photographs and LiDAR intensity images.

Figure 3. Example of co-registration of color images with LiDAR intensity images.

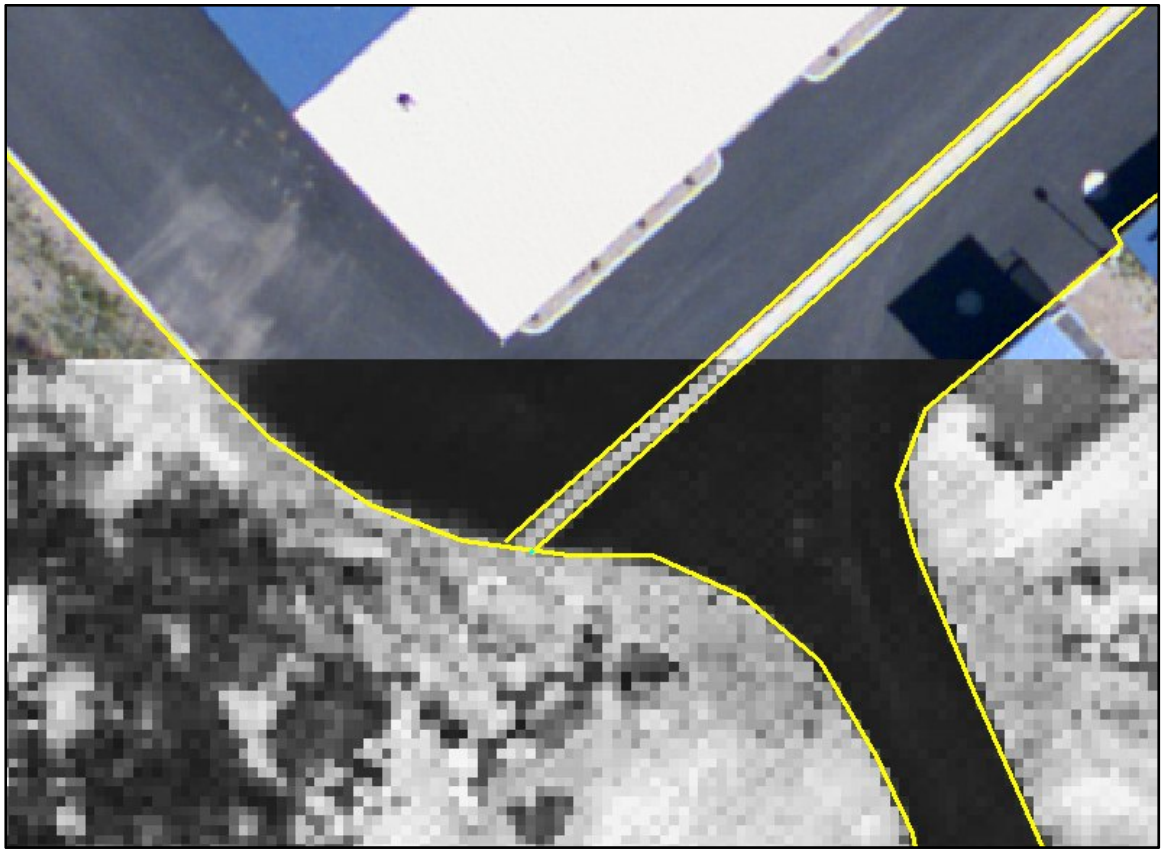

6. Study Area Results

Summary statistics for point resolution and accuracy (relative and absolute) of the LiDAR data collected in the Walla Walla River survey area are presented below in terms of central tendency, variation around the mean, and the spatial distribution of the data (for point resolution by bin). The delivered dataset meets or exceeds specifications for resolution and accuracy as outlined in the contract (Table 2).

6.1 Data Summary

Table 2. LiDAR Resolution and Accuracy - Specifications and Achieved Values

	Targeted	Achieved
Resolution:	≥ 8 points/m^2	8.17 points/m^2
***Vertical Accuracy (1 σ):**	≤15 cm	3.0 cm

6.2 LiDAR Point Density/Resolution

The average data density across the Walla Walla River survey area exceeded the targeted resolution. Density values will vary throughout the project area, it is not uncommon for some types of surfaces (e.g. dense vegetation, agricultural fields, and water) to return fewer pulses than the laser originally emitted. These discrepancies between 'native' and 'delivered' density will vary depending on terrain, land cover and the prevalence of water bodies.

Ground classifications were derived from automated ground surface modeling and manual, supervised classifications where it was determined that the automated model had failed. Ground return densities will be lower in areas of dense vegetation, water, or buildings.

Figure 4 (below) displays the spatial distribution of first-return and ground-classified point densities per processing tile.

Figure 4. Density distribution for ground-return and first-return laser points per processing bin

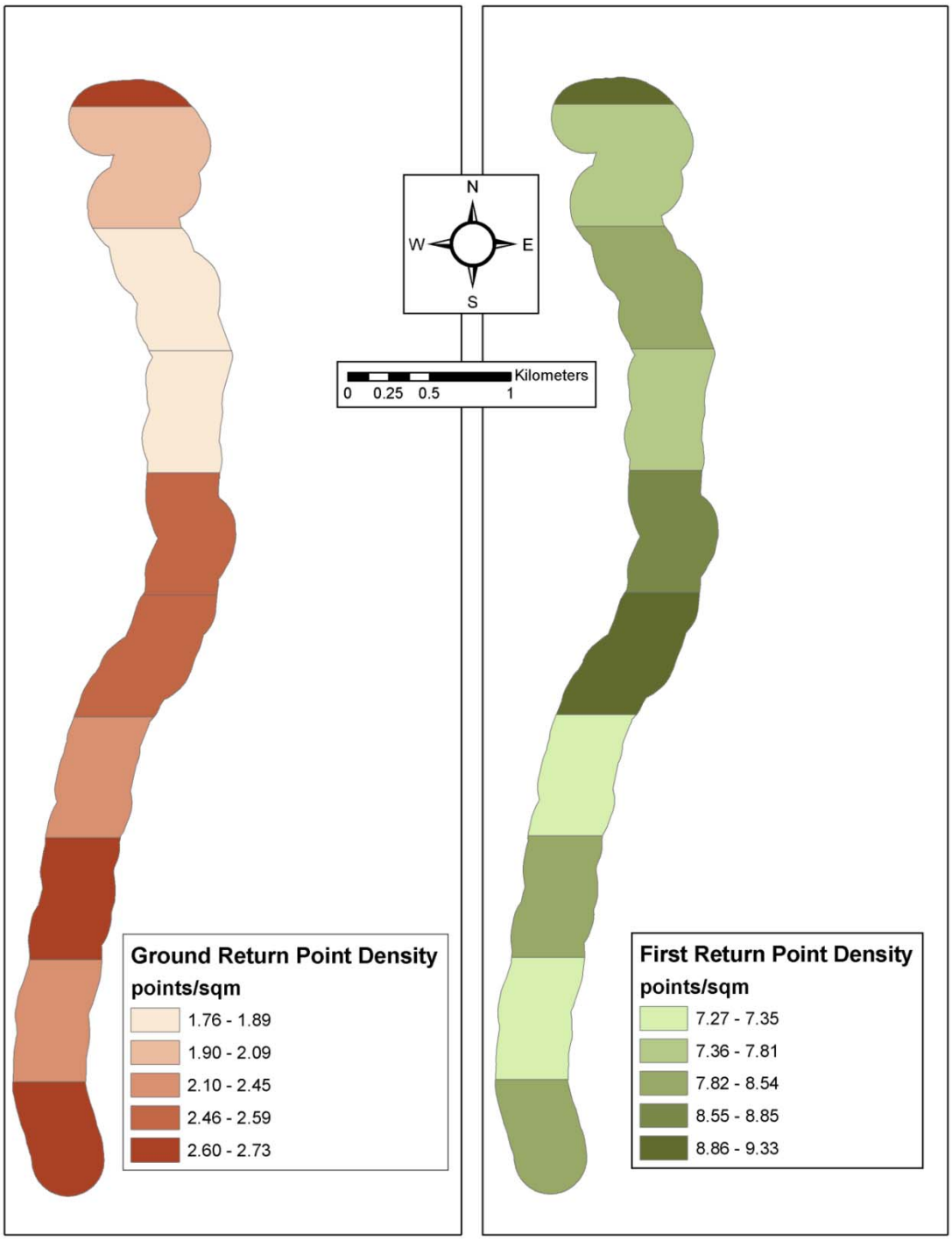

LiDAR data resolution for the Walla Walla River, OR/WA survey area:

- Average Point (First Return) Density = 8.17 points/m^2
- Average Ground Point Density = 2.34 points/m^2

Figure 5. Density distribution for first return laser points

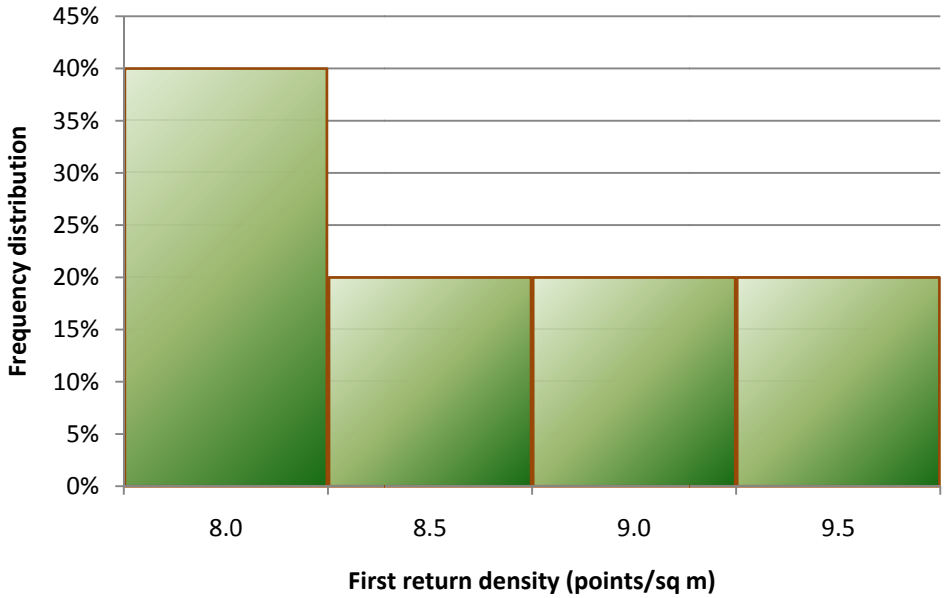

Figure 6. Density distribution for ground-classified laser points

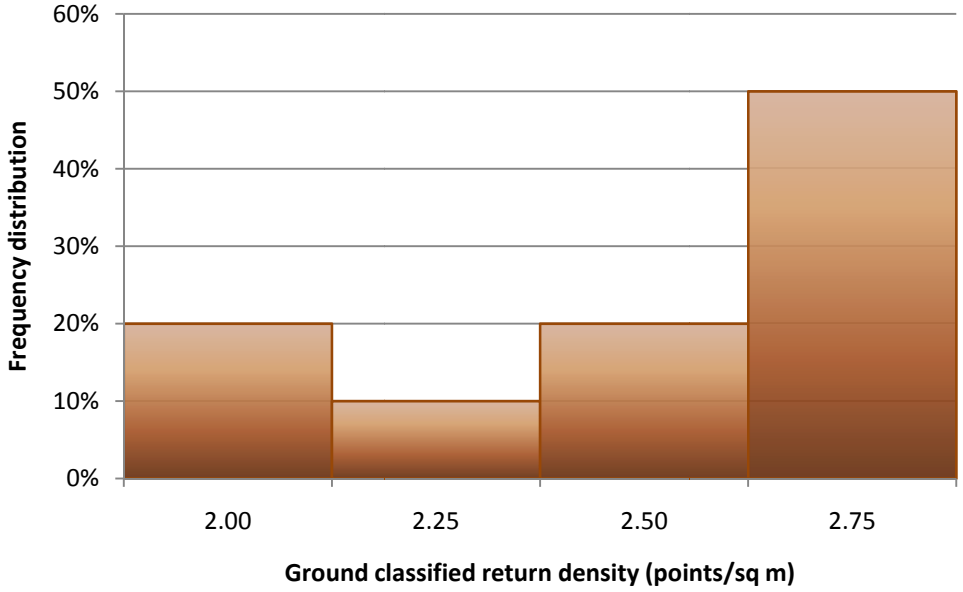

6.3 LiDAR Relative Accuracy Calibration Results

Relative accuracies for the Walla Walla River, OR/WA survey areas:

- Project Average = 0.027m
- Median Relative Accuracy = 0.027m
- 1σ Relative Accuracy = 0.027m
- 2σ Relative Accuracy = 0.032m

Figure 7. Distribution of relative accuracies per flight line, non slope-adjusted

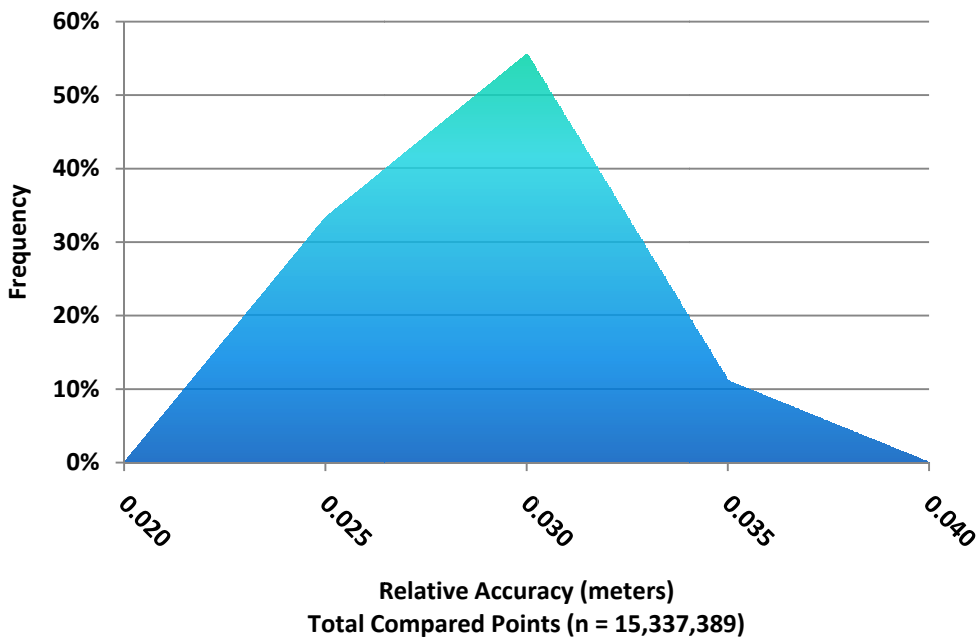

6.4 LiDAR Absolute Accuracy

Absolute accuracies for the Walla Walla River, OR/WA survey area

Table 3. Absolute Accuracy – Deviation between laser points and RTK hard surface survey points

RTK Survey Sample Size (n): 252	
Root Mean Square Error (RMSE) = 0.04m	Minimum Δz = -0.11m
Standard Deviations 1 sigma (σ): 0.03m 2 sigma (σ): 0.07m	Maximum Δz = 0.09m Average Δz = 0.00m

Figure 8. Absolute Accuracy - Histogram Statistics, based on hard surface points

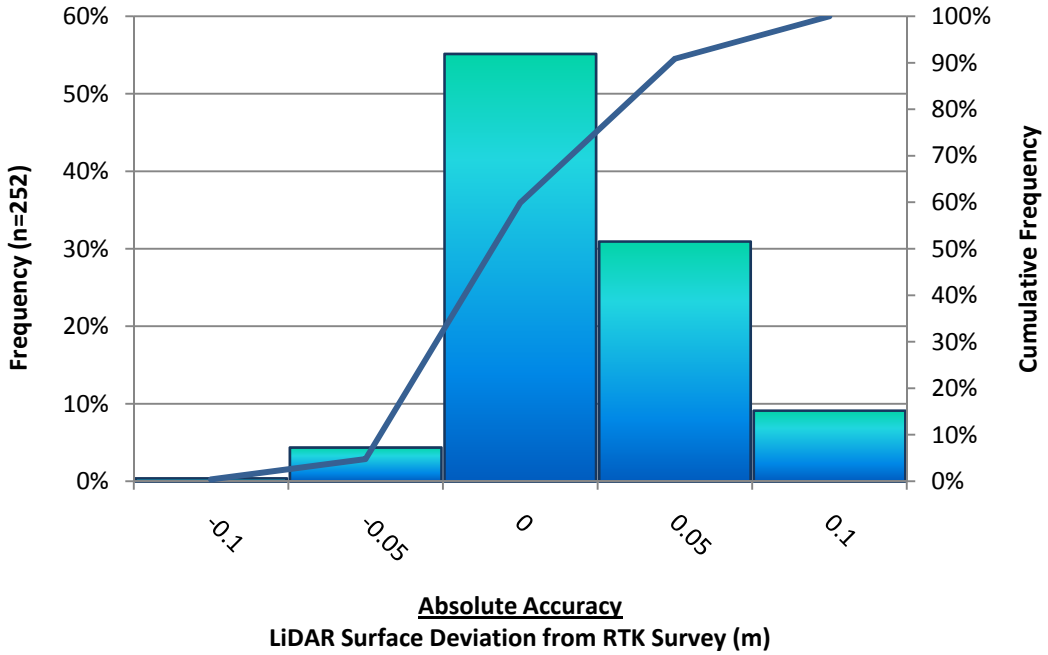

Figure 9. Absolute Accuracy - Absolute Deviation, based on 252 hard surface points

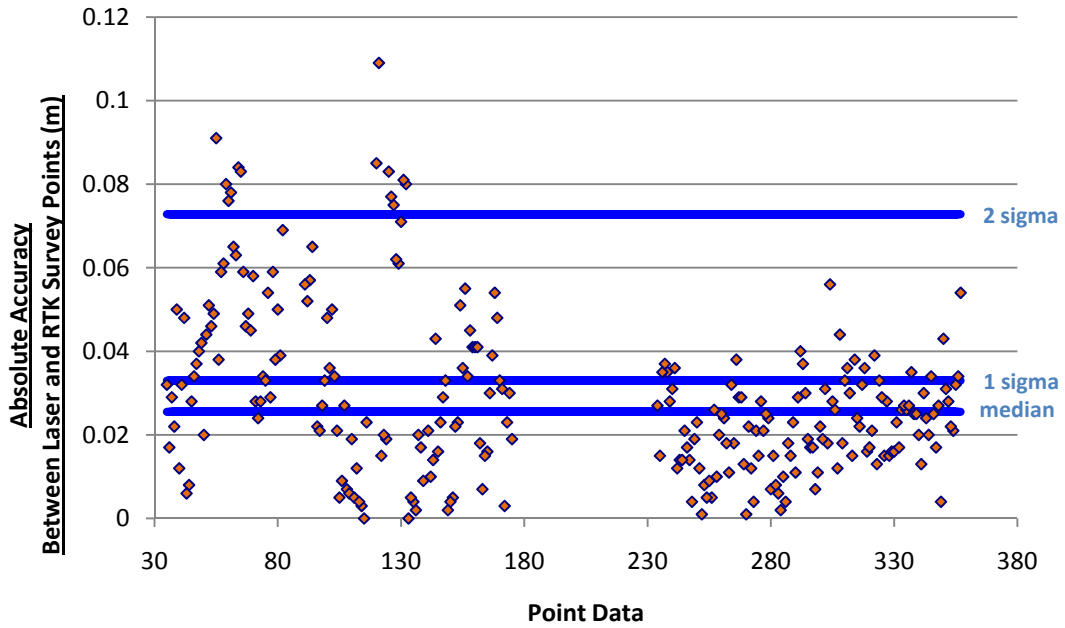

6.5 Orthophotograph Accuracy

Aerial imagery accuracy for the Walla Walla River survey area are found in figures 10 and 11 below and table 4 below.

Figure 10. Orthophoto bin delineations for the Walla Walla survey area displayed with accuracy checkpoints.

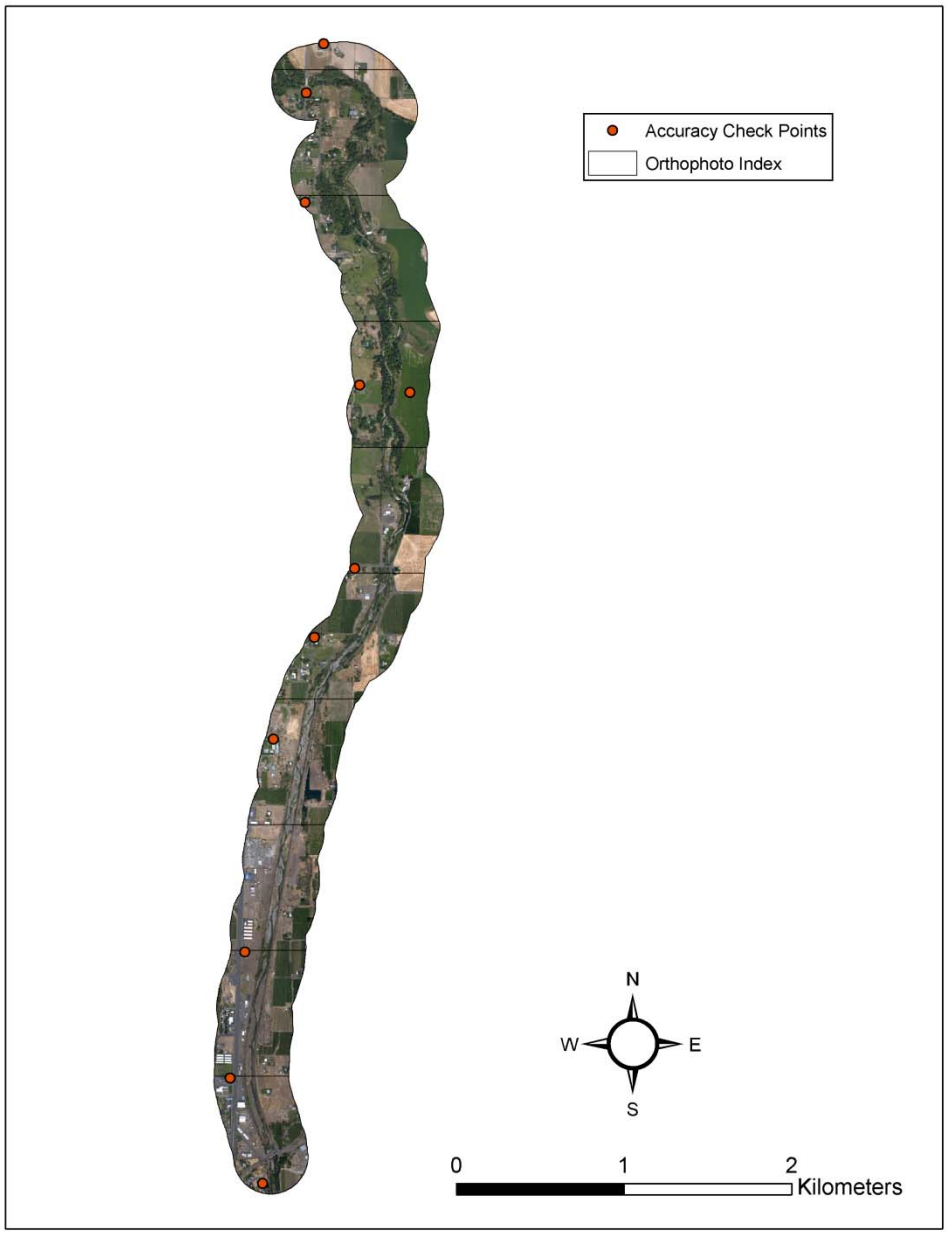

Table 4. Deviation between aerial photos and intensity images based on 11 accuracy check points.

	Mean	Standard Deviation (1 Sigma)	Root Mean Square Error (RMSE)
Walla Walla Photos	0.01m	0.10m	0.10m

Figure 11. Checkpoint residuals derived from comparing aerial photos to intensity images

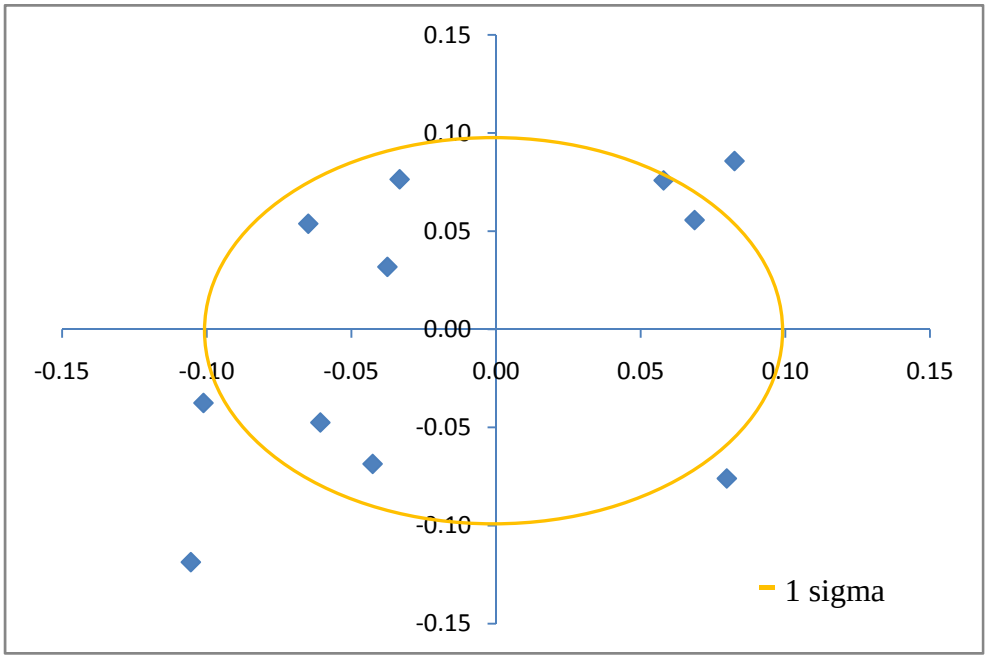

6.6 Projection/Datum and Units

	Projection:	UTM Zone 11 North, NAD 83
Datum	**Vertical:**	NAVD88 Geoid03
	Horizontal:	NAD83
	Units:	meters

7. Deliverables

Point Data:	• All laser return points (LAS v. 1.1 format)
Vector Data:	• LiDAR tile index (shapefile format)
Raster Data:	• Intensity Images (0.5 m GeoTIFF format; 1/100th quad delineation) • Bare-Earth Model (1 m ESRI GRID format; 1/4th USGS quad delineation) • Highest-Hit Model (1 m ESRI GRID format; 1/4th USGS quad delineation) • Orthorectified True Color Imagery (GeoTIFF format, 10cm resolution)
Data Report:	• Full Report containing introduction, methodology, and accuracy

8. Selected Images

Figure 12. Point cloud image derived from LiDAR data facing southwest looking at Eastside road.

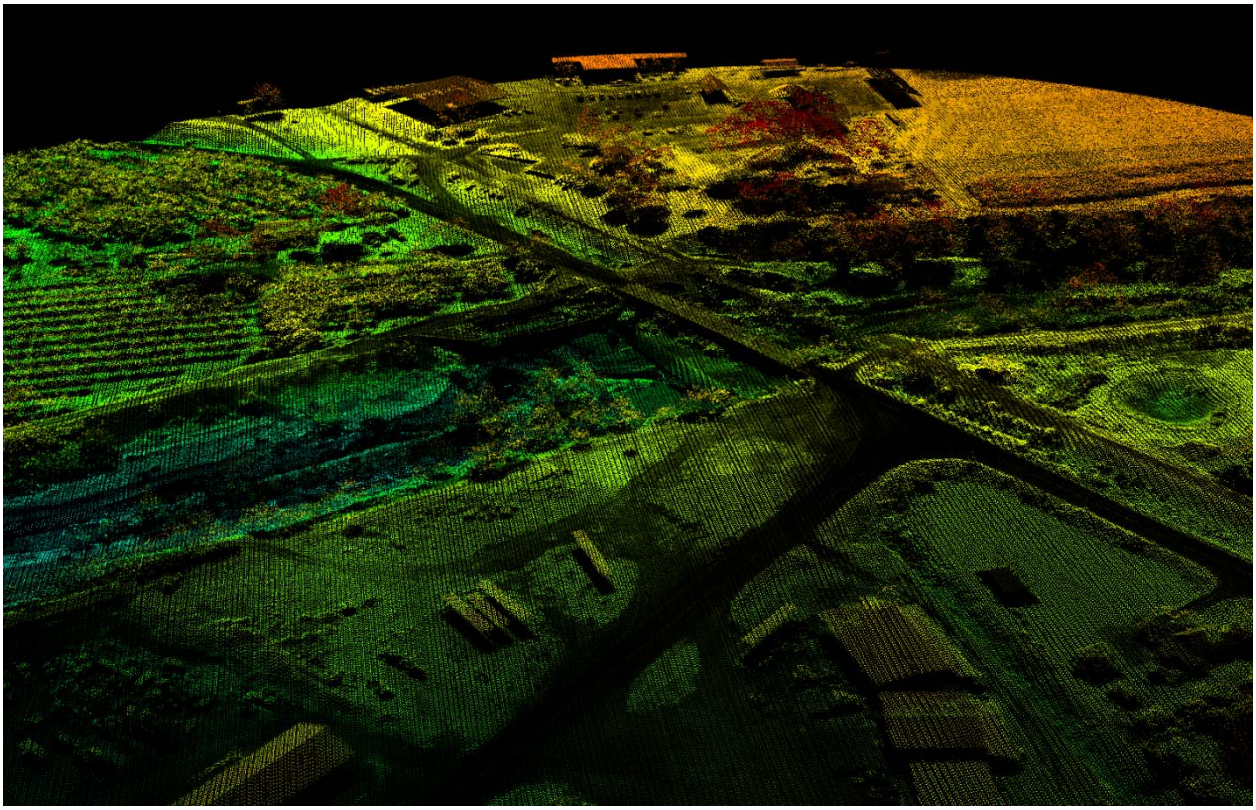

Figure 13. Point cloud image derived from LiDAR data looking northeast in the Walla Walla study area.

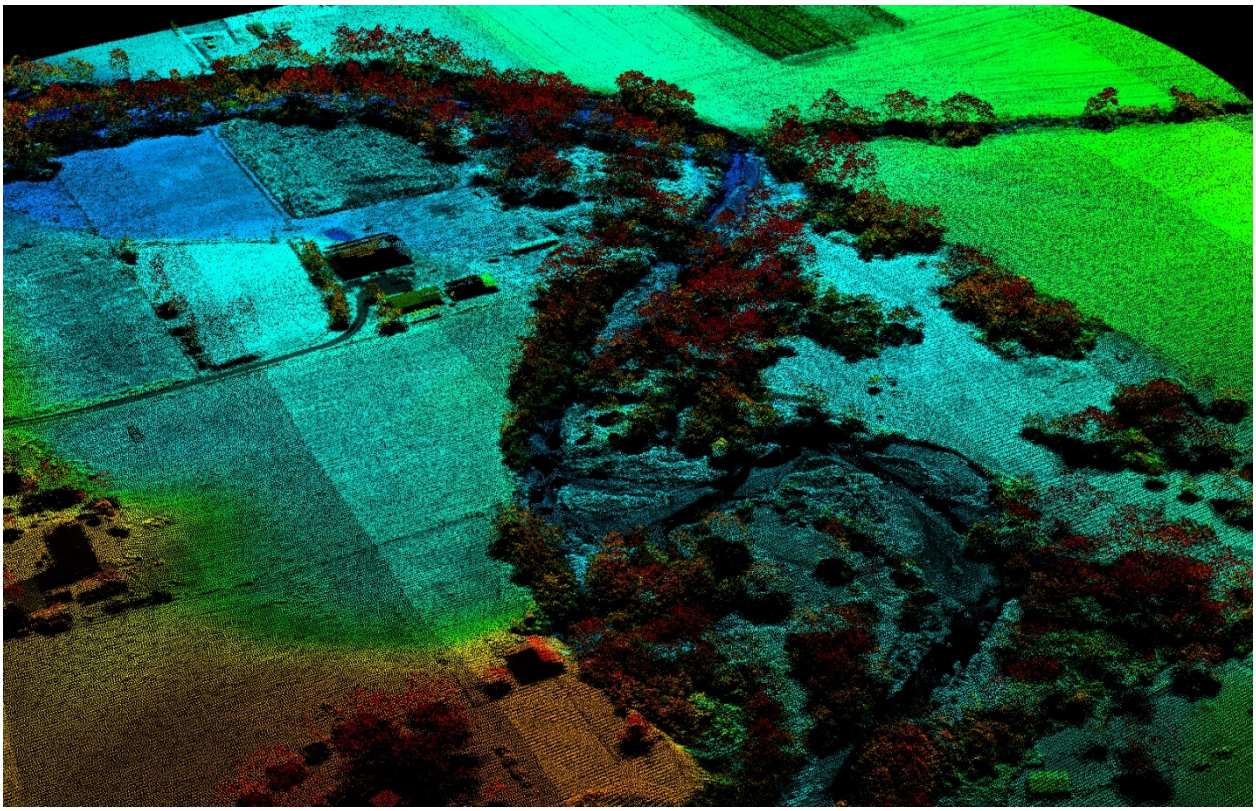

Figure 14. The top image is a 3d view of the north eastern portion of Walla Walla River study area with ortho imagry draped over highest hit LiDAR. The bottom image is a bare earth model that isderived from ground classified LiDAR points.

9. Glossary

1-sigma (σ) Absolute Deviation: Value for which the data are within one standard deviation (approximately 68th percentile) of a normally distributed data set.

2-sigma (σ) Absolute Deviation: Value for which the data are within two standard deviations (approximately 95th percentile) of a normally distributed data set.

Root Mean Square Error (RMSE): A statistic used to approximate the difference between real-world points and the LiDAR points. It is calculated by squaring all the values, then taking the average of the squares and taking the square root of the average.

Pulse Rate (PR): The rate at which laser pulses are emitted from the sensor; typically measured as thousands of pulses per second (kHz).

Pulse Returns: For every laser pulse emitted, the Leica ALS 50 Phase II system can record *up to four* wave forms reflected back to the sensor. Portions of the wave form that return earliest are the highest element in multi-tiered surfaces such as vegetation. Portions of the wave form that return last are the lowest element in multi-tiered surfaces.

Accuracy: The statistical comparison between known (surveyed) points and laser points. Typically measured as the standard deviation (sigma, σ) and root mean square error (RMSE).

Intensity Values: The peak power ratio of the laser return to the emitted laser. It is a function of surface reflectivity.

Data Density: A common measure of LiDAR resolution, measured as points per square meter.

Spot Spacing: Also a measure of LiDAR resolution, measured as the average distance between laser points.

Nadir: A single point or locus of points on the surface of the earth directly below a sensor as it progresses along its flight line.

Scan Angle: The angle from nadir to the edge of the scan, measured in degrees. Laser point accuracy typically decreases as scan angles increase.

Overlap: The area shared between flight lines, typically measured in percents; 100% overlap is essential to ensure complete coverage and reduce laser shadows.

DTM / DEM: These often-interchanged terms refer to models made from laser points. The digital elevation model (DEM) refers to all surfaces, including bare ground and vegetation, while the digital terrain model (DTM) refers only to those points classified as ground.

Real-Time Kinematic (RTK) Survey: GPS surveying is conducted with a GPS base station deployed over a known monument with a radio connection to a GPS rover. Both the base station and rover receive differential GPS data and the baseline correction is solved between the two. This type of ground survey is accurate to 1.5 cm or less.

10. Citations

Soininen, A. 2004. TerraScan User's Guide. TerraSolid.

Appendix A

LiDAR accuracy error sources and solutions:

Type of Error	Source	Post Processing Solution
GPS (Static/Kinematic)	Long Base Lines	None
	Poor Satellite Constellation	None
	Poor Antenna Visibility	Reduce Visibility Mask
Relative Accuracy	Poor System Calibration	Recalibrate IMU and sensor offsets/settings
	Inaccurate System	None
Laser Noise	Poor Laser Timing	None
	Poor Laser Reception	None
	Poor Laser Power	None
	Irregular Laser Shape	None

Operational measures taken to improve relative accuracy:

1. Low Flight Altitude: Terrain following is employed to maintain a constant above ground level (AGL). Laser horizontal errors are a function of flight altitude above ground (i.e., ~ 1/3000th AGL flight altitude).
2. Focus Laser Power at narrow beam footprint: A laser return must be received by the system above a power threshold to accurately record a measurement. The strength of the laser return is a function of laser emission power, laser footprint, flight altitude and the reflectivity of the target. While surface reflectivity cannot be controlled, laser power can be increased and low flight altitudes can be maintained.
3. Reduced Scan Angle: Edge-of-scan data can become inaccurate. The scan angle was reduced to a maximum of ±14° from nadir, creating a narrow swath width and greatly reducing laser shadows from trees and buildings.
4. Quality GPS: Flights took place during optimal GPS conditions (e.g., 6 or more satellites and PDOP [Position Dilution of Precision] less than 3.0). Before each flight, the PDOP was determined for the survey day. During all flight times, a dual frequency DGPS base station recording at 1–second epochs was utilized and a maximum baseline length between the aircraft and the control points was less than 19 km (11.5 miles) at all times.
5. Ground Survey: Ground survey point accuracy (i.e. <1.5 cm RMSE) occurs during optimal PDOP ranges and targets a minimal baseline distance of 4 miles between GPS rover and base. Robust statistics are, in part, a function of sample size (n) and distribution. Ground survey RTK points are distributed to the extent possible throughout multiple flight lines and across the survey area.
6. 50% Side-Lap (100% Overlap): Overlapping areas are optimized for relative accuracy testing. Laser shadowing is minimized to help increase target acquisition from multiple scan angles. Ideally, with a 50% side-lap, the most nadir portion of one flight line coincides with the edge (least nadir) portion of overlapping flight lines. A minimum of 50% side-lap with terrain-followed acquisition prevents data gaps.
7. Opposing Flight Lines: All overlapping flight lines are opposing. Pitch, roll and heading errors are amplified by a factor of two relative to the adjacent flight line(s), making misalignments easier to detect and resolve.

Appendices II:

Memorandum

Date: April 24, 2009

To: Bob Bower, Walla Walla Basin Watershed Council
John Selker, Oregon State University

From: Landon Gryczkowski, Oregon State University
Email: Gryczkol@onid.orst.edu

Subject: Electrical resistivity in the Walla Walla basin

The purpose of this memo is to explain how electrical resistivity profiles can benefit the scientific objectives of ongoing work in the Walla Walla basin and to propose the use of electrical resistivity surveys in the 2009 field season.

Electrical resistivity overview

Electrical resistivity is a non-invasive geophysical method for exploring the shallow subsurface by applying current at the ground surface and measuring the potential difference between two points. A resistivity array or profile provides a two or three-dimensional image of the resistivity distribution in the subsurface. Variations in resistance to current flow at depth cause distinctive variations in potential difference, allowing for the interpretation of subsurface materials and structure.

Geophysics for hydrology

Recent technological advances in resistivity equipment and data analysis software have expanded the use and applicability of resistivity surveys to hydrologic studies and investigations. Recognizing this, the Consortium of Universities for Advancement of Hydrologic Science, Inc. (CUAHSI) recently developed a geophysics module within the Hydrologic Measurement Facility (HMF) to support and advance the use of geophysics for hydrologic applications.

The USGS Office of Groundwater, Branch of Geophysics has conducted a variety of hydrologic studies using resistivity, particularly continuous resistivity profiling in the past several years. Links to USGS publications are included below the “references and links” heading. Continuous resistivity profiling involves the towing of floating electrodes behind a boat, allowing the collection of ten to twenty kilometers of data per day. Among some of the identified uses of continuous resistivity profiling data as identified by the USGS include mapping freshwater seeps, imaging the saltwater/freshwater interface, developing a hydrogeologic framework, delineating sediment types, and mapping contamination plumes. A few studies have specifically used resistivity surveys to investigate surface water/groundwater interaction and hyporheic exchange to better understand river processes.

Application to objectives in the Walla Walla basin

High resolution resistivity imaging of the subsurface beneath the Walla Walla River would complement and validate the data provided by the fiber optic distributed temperature sensing system (DTS). Additionally, the use of DTS may serve as a validation tool for resistivity surveys. The pairing of DTS with resistivity would provide more information than either method alone and may open windows to a reasonable method of obtaining detailed, high resolution data to characterize and investigate river processes. Resistivity surveys can provide indications of relative grain sizes and porosity of alluvial subsurface materials, thus identifying preferential flowpaths, historical channels, areas of varying infiltration potential, and specific locations of increased potential flux of water through the stream bed. Additionally, depending on the specific array used, the depth to basalt can be determined. This information can then be compared to data from the DTS as validation and also to investigate correlations between resistivity and temperature anomalies as observed by the DTS. These correlations may provide a means of explaining why hyporheic exchange and groundwater discharge occur where they are observed by the DTS. Also, if strong correlations are found, additional resistivity profiles can be obtained from other river reaches in the basin to predict gains, losses, hyporheic exchange, and areas of specific management concern. Data from resistivity surveys can also be compared to previous work on the project, specifically the work of Starr Metcalf in the 2001 and 2002 field seasons in relation to the extrapolation of point measurements to entire reaches.

Since resistivity can detect changes in the specific conductance of water, surface water/groundwater mixing may be able to be detected based on the differing specific conductance of surface water and groundwater, somewhat similar to the mapping of saltwater/freshwater interfaces in previous studies. However, the differences may be too small to detect and it may require continuous monitoring over time to differentiate between changes in specific conductance and changes in physical subsurface structure. The use of salt tracers may allow for the monitoring and detection of hyporheic flowpaths through resistivity imaging, providing information on the depth of hyporheic exchange, travel and residence times, and processes governing the flux of water through the river bed.

Proposed plans for summer of 2009

A waterborne resistivity survey is proposed in the Walla Walla River by laying a submersible cable of electrodes along a fiber optic cable on the river bed and using the “slide-along” method to traverse the entire reach. This will be performed along each fiber optic cable. The slide-along method is able to obtain better quality data than the towing of floating electrodes at the expense of longer data collection time. A few kilometers of data can be collected per day using the slide-along method. To investigate relationships between lateral flow of water and resistivity, traditional land-based profiles are proposed in the riparian zones.

USGS support

Dr. Fred Day-Lewis from the USGS Office of Groundwater, Branch of Geophysics is an expert with the use of modern resistivity techniques for hydrologic applications as well as DTS and has shown enthusiastic support for the proposal to pair DTS with resistivity imaging in the

Walla Walla River. He and his colleagues have shown interest in collaboration in the effort, and have offered to send a geophysicist from their office to the field site to perform the resistivity surveys and also to analyze the resulting data. The USGS has provided an estimated cost of $15 – 20,000 for a week of field work and a week of data analysis. USGS involvement will ensure that the data are collected and analyzed properly and professionally and will make the project and results more reputable.

References and links

Ball, L.B., W.H. Kress, G.V. Steele, J.C. Cannia, and M.J. Andersen. 2006. Determination of Canal Leakage Potential Using Continuous Resistivity Profiling Techniques, Interstate and Tri-State Canals, Western Nebraska and Eastern Wyoming, 2004: U.S. Geological Survey Scientific Investigations Report 2006 – 5032, 53 p.
http://pubs.usgs.gov/sir/2006/5032/pdf/sir2006-5032.pdf

Belaval, M., J.W. Lane, Jr., D.P. Lesmes, and G.C. Kineke. 2003. Continuous-resistivity profiling for coastal groundwater investigations: three case studies, in Symposium on the Application of Geophysics to Engineering and Environmental Problems (SAGEEP), April 6-10, 2003, San Antonio, Texas, Proceedings: Denver, Colorado, Environmental and Engineering Geophysical Society, CD-ROM, 14 p.
http://water.usgs.gov/ogw/bgas/publications/SAGEEP03_Belaval/SAGEEP03_Belaval.pdf

Consortium of Universities for Advancement of Hydrologic Science, Inc. Hydrologic Measurement Facility: Geophysics.
http://www.cuahsi.org/hmf/geo-index.html

Crook, N., A. Binley, R. Knight, D. A. Robinson, J. Zarnetske, and R. Haggerty. 2008. Electrical resistivity imaging of the architecture of substream sediments, *Water Resour. Res*., 44, W00D13, doi:10.1029/2008WR006968.
http://www.agu.org/pubs/crossref/2008/2008WR006968.shtml

Henderson, R.D., F.D. Day-Lewis, J.W. Lane, Jr., C.F. Harvey, and L.Liu. 2008. Characterizing submarine ground-water discharge using fiber-optic distributed temperature sensing and marine electrical resistivity, in Symposium on the Application of Geophysics to Engineering and Environmental Problems, April 6-10, 2008, Philadelphia, Pennsylvania, Proceedings: Denver, Colorado, Environmental and Engineering Geophysical Society, 11p.
http://water.usgs.gov/ogw/bgas/publications/SAGEEP2008-Henderson/SAGEEP2008-Henderson.pdf

Johnson, C.D., and E.A. White. 2007. Marine geophysical investigation of selected sites in Bridgeport, Harbor, Connecticut, 2006: U. S. Geological Survey Scientific Investigations Report 2007–5119, 32 p., online only.
http://pubs.usgs.gov/sir/2007/5119/

Robinson, D.A., A. Binley, N. Crook, F.D. Day-Lewis, T.P.A. Ferre, V.J.S. Grauch, R. Knight, M. Knoll, V. Lakshmi, R. Miller, J. Nyquist, L. Pellerin, K. Singha, and L. Slater. 2006. A Vision for Geophysics Instrumentation in Watershed Hydrological Research. A Report to the Consortium of Universities for the Advancement of Hydrologic Sciences, Inc.
http://www.cuahsi.org/hmf/docs/geophysics-20061031.pdf

Robinson, D.A., A. Binley, N. Crook, F.D. Day-Lewis, T.P.A. Ferre, V.J.S. Grauch, R. Knight, M. Knoll, V. Lakshmi, R. Miller, J. Nyquist, L. Pellerin, K. Singha, and L. Slater. 2008. Advancing process-based watershed hydrological research using near-surface geophysics: a vision for, and review of, electrical and magnetic geophysical methods. *Hydrologic Processes*, doi:10.1002/hyp.6963, 32p.
http://water.usgs.gov/ogw/bgas/publications/HP2008-Robinson/

Teeple, A., A.K. McDonald, W. Kress. 2007. Assessment of streambed heterogeneity along a segment of the Upper Pecos River, Mentone, Texas. Joint Rio Grande Basin Initiatives Annual Conference, May, 2007.
http://riogrande-conference.tamu.edu/wrapup/2007/posters/teeple.pdf

U.S. Geological Survey, Office of Groundwater, Branch of Geophysics. 2006. Profiles in Geophysics: Niantic River, CT - Continuous Resistivity Profiling Project.
http://water.usgs.gov/ogw/bgas/profiles/Feb2006-CRP.html

U.S. Geological Survey, Office of Groundwater, Branch of Geophysics. 2007. Continuous resistivity profiling.

http://water.usgs.gov/ogw/bgas/crp/

Zarnetske, J.P., R. Haggerty , N. Crook , and D.R. Robinson. 2006. Hyporheic geophysics: D.C. resistivity imaging of valley-bottom alluvium in a 3rd-order mountain stream, HJ Andrews Experimental Forest, Oregon, USA. Eos Trans. AGU, Fall Meet. Suppl. http://oregonstate.edu/~zarnetsj/Pubs_Present_pdfs/HZNO3geophys_AGUFL06_JPZ_vfinal.pdf

Example resistivity images

From Teeple et al. (2007):

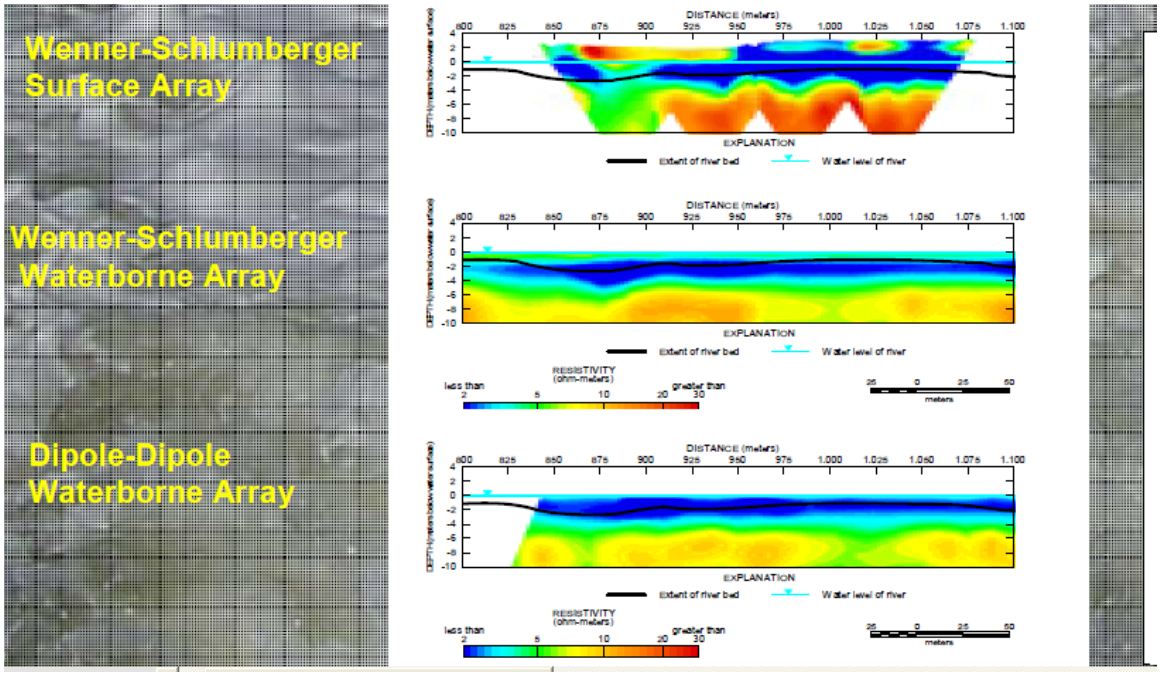

Waterborne Array Results

Wenner-Schlumberger array

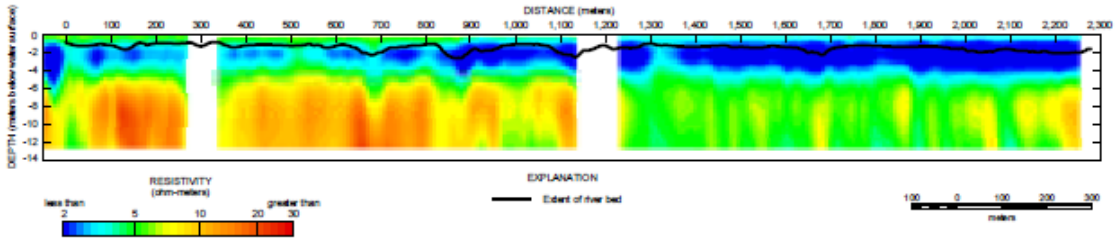

Dipole-dipole array

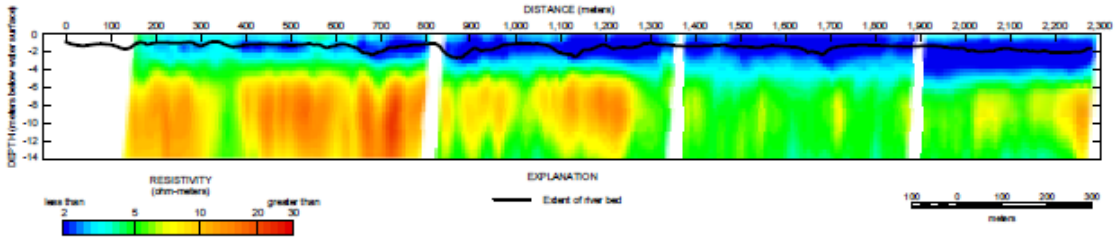

From Belaval et al. (2003):

Winyah Bay, 2002, Resistivity Profiles WB18 and WB21

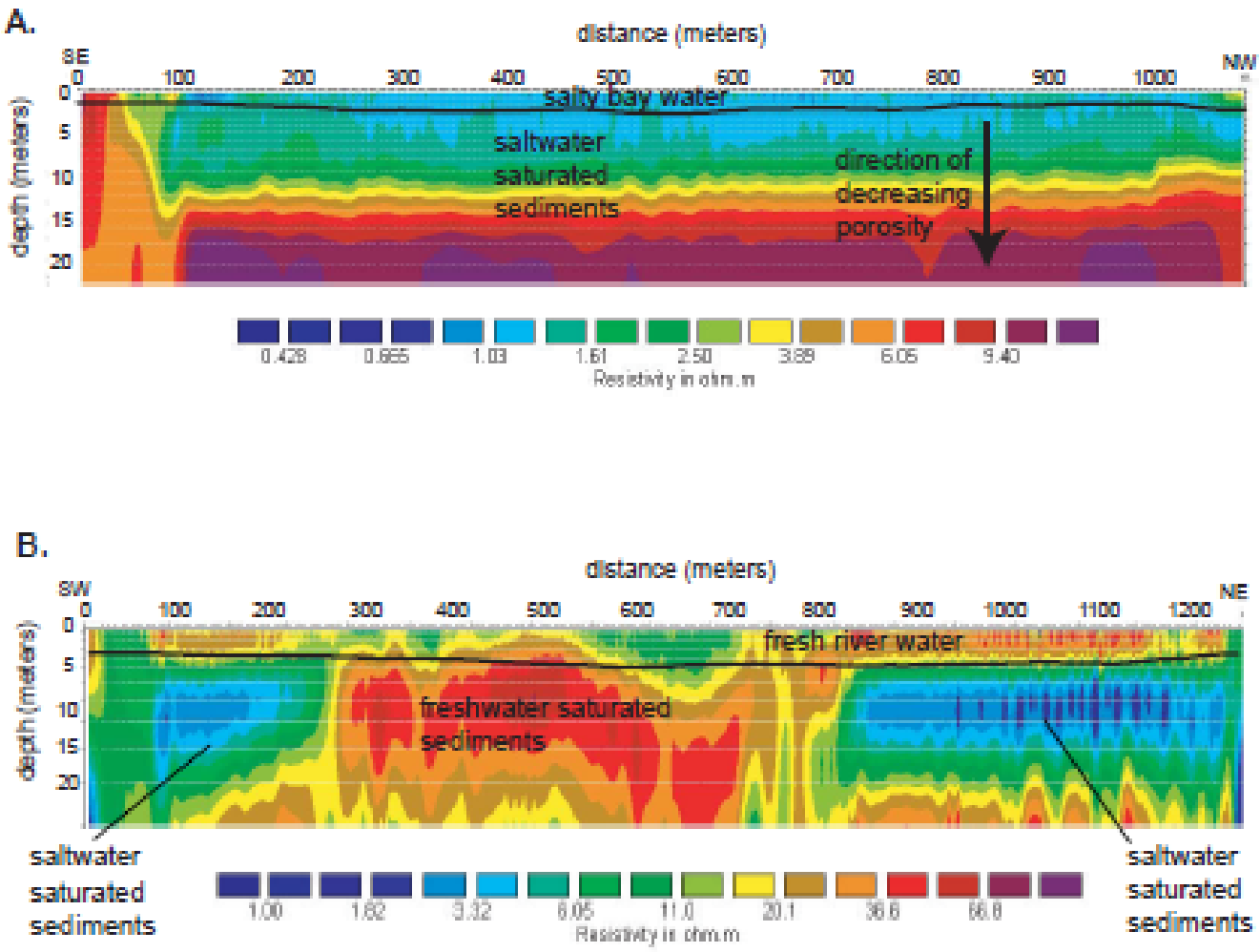

Figure 2. Inverted resistivity section WB18 with interpretations (A) and WB21 with interpretations (B). The inverted model displayed for WB18 is the third iteration with a root mean squared error (RMSE) of 3.3%. The inverted model displayed for WB21 is the fifth iteration with an RMSE of 4.3%. Water bottom measured by an echo sounder is plotted as a dark line.

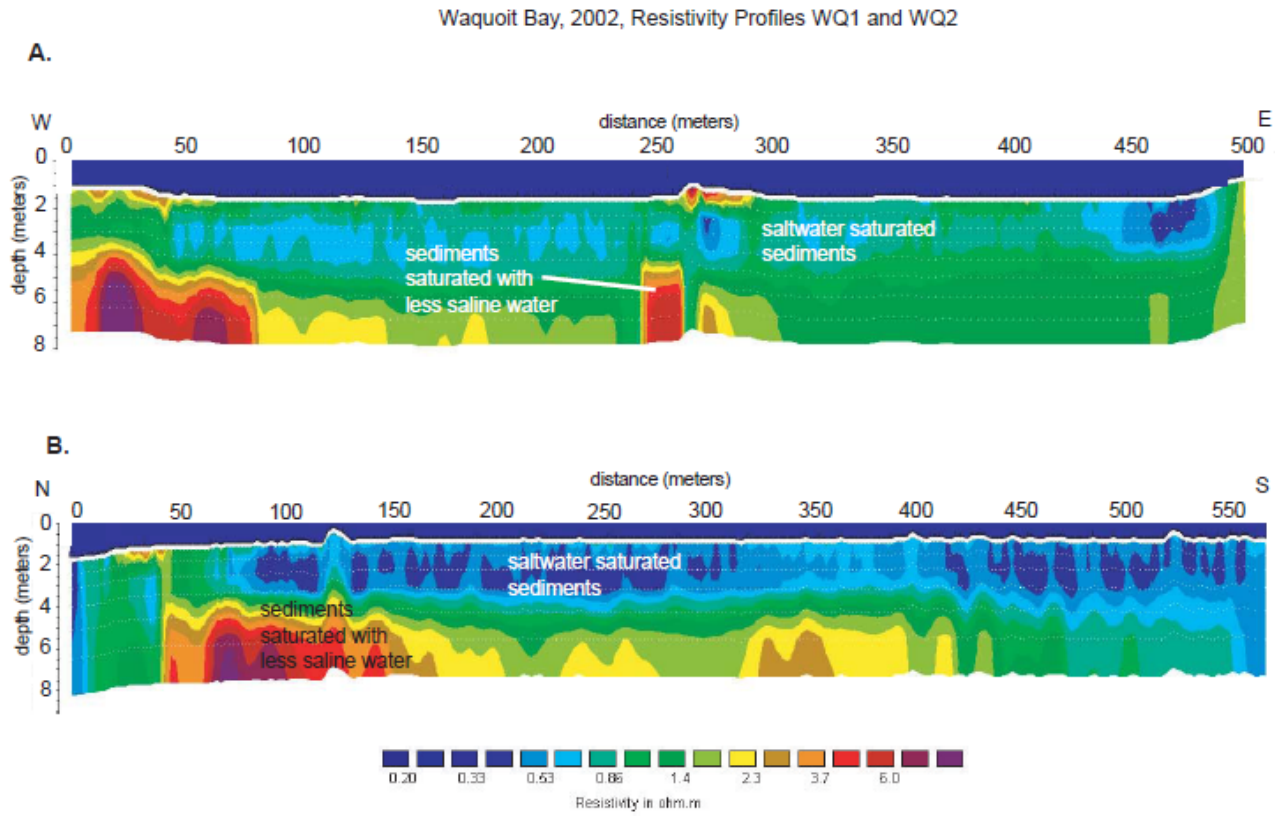

Figure 6. Inverted resistivity section WQ1 (A) (alongshore) and WQ2 (B) (offshore). The inverted model displayed for WQ1 is the third iteration with a root mean squared error (RMSE) of 2.9%. The inverted model displayed for WQ2 is the third iteration with an RMSE of 4.6%. Both sections have been inverted with the water column resistivity constained to 0.25 ohm-meter. A white line marks the water bottom as recorded by an echo sounder.

From Johnson and White (2007):

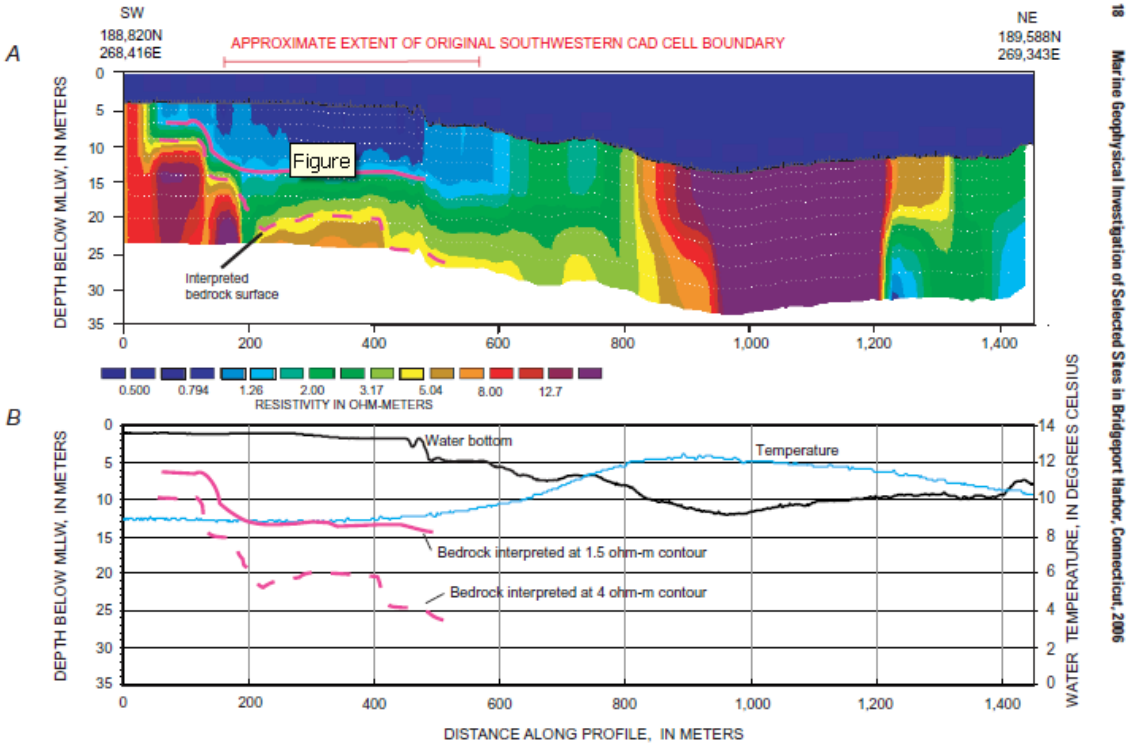

Figure 6. Continuous resistivity survey from Profile 1, Bridgeport Harbor, Bridgeport, Connecticut, showing (*A*) the inverted, constrained data, and (*B*) the interpretation of depth to bedrock, measured depth to water bottom, and temperature of near-surface water in degrees Celsius. The solid and dashed red lines show the interpreted bedrock surface. Depths are shown in meters below the mean low-low water (MLLW) surface. Profile runs southwest to northeast. End-point positions are in Connecticut State Plane Coordinate System using the North American Datum of 1983, in meters.

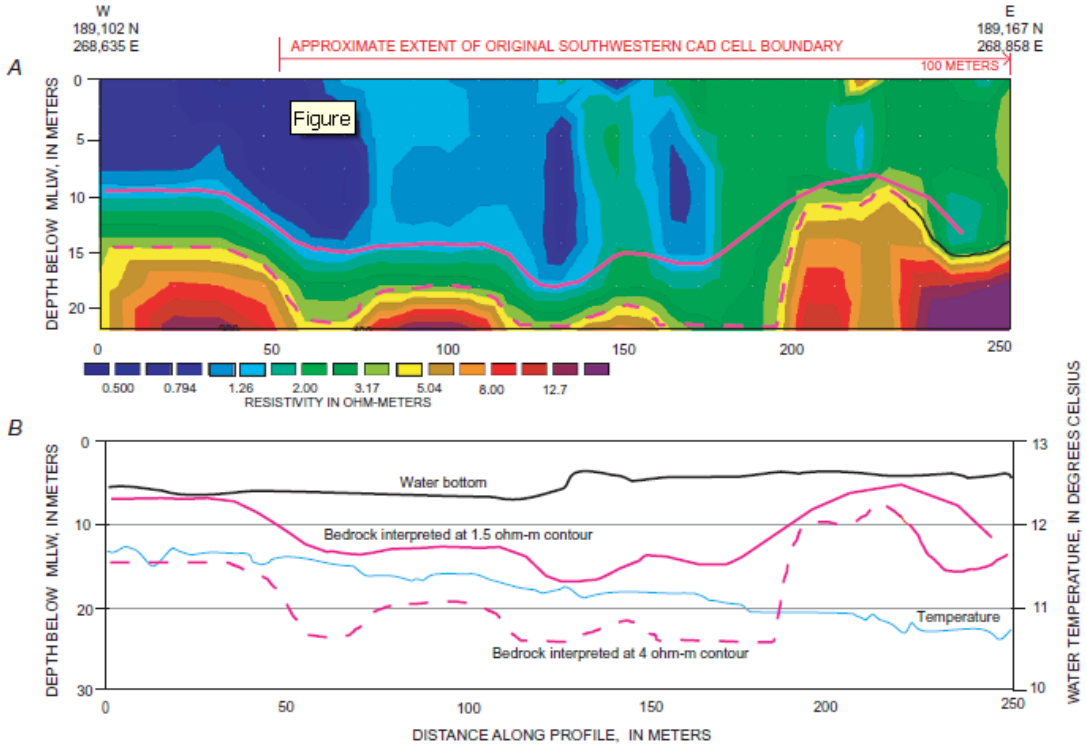

Figure 8. Continuous resistivity survey from western end of Profile 2, Bridgeport Harbor, Bridgeport, Connecticut, showing (*A*) the unconstrained, robust inversion, and (*B*) the interpretation of depth to bedrock, measured depth to water bottom, and temperature of near-surface water in degrees Celsius. Depths are shown in meters below the mean low-low water (MLLW). The original southwestern CAD cell extends about 100 meters to the east of the profile. End-point positions are in Connecticut State Plane Coordinate System using the North American Datum of 1983, in meters.

From Ball et al. (2006):

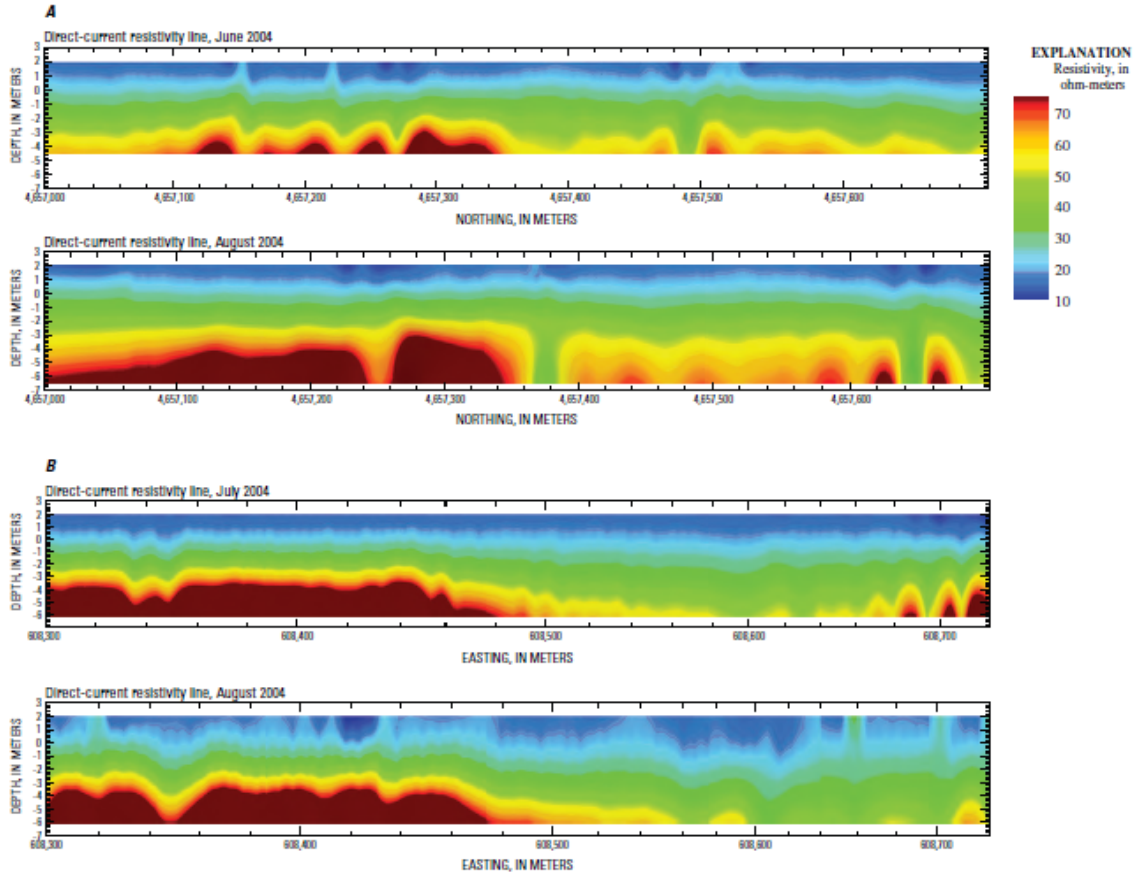

Figure 30. Co-located water-borne direct-current resistivity sections collected in ***A***, June and August 2004 in the Interstate Canal, and ***B***, July and August in the Tri-State Canal.

From Robinson et al. (2008):

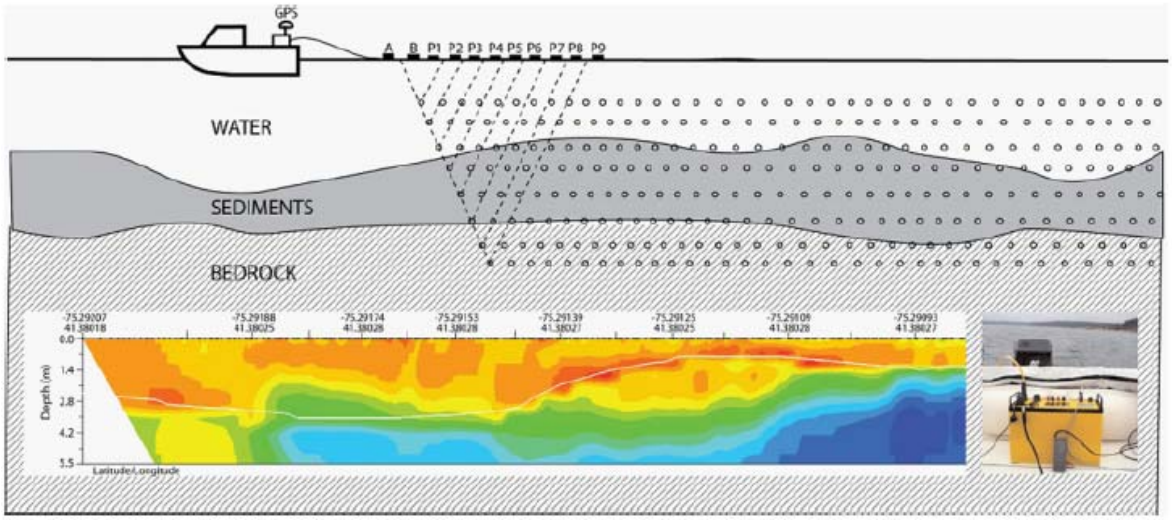

Figure 14. Multi-electrode cable towed by boat with GPS positioning and example resistivity profile (left); the resistivity instrument is shown on the right

From U.S. Geological Survey, Office of Groundwater, Branch of Geophysics (2007):

Sample Inverted CRP Model

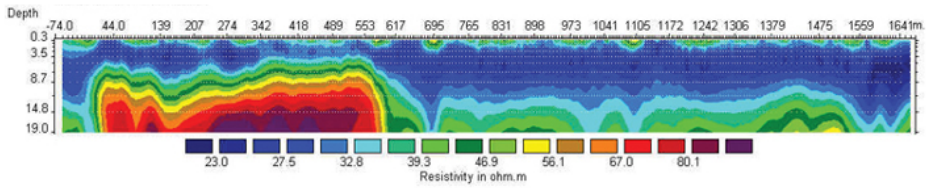

Inverted resistivity model from Lake Travis, Austin, Texas. Cooler colors represent regions of lower resistivity, and warmer colors represent regions of higher resistivity. The water-bottom begins in the blue-to-green resistivity zones. Due to the motion of the boat, the effective spacing between electrodes is estimated to be 1 meter. The inverted resistivity model is shown after 3 iterations, with a root-mean-square error of 3.7 percent.

Sample CRP Field Data and Inverted Models: Effects of Constraints on Water Column in Inversion Process

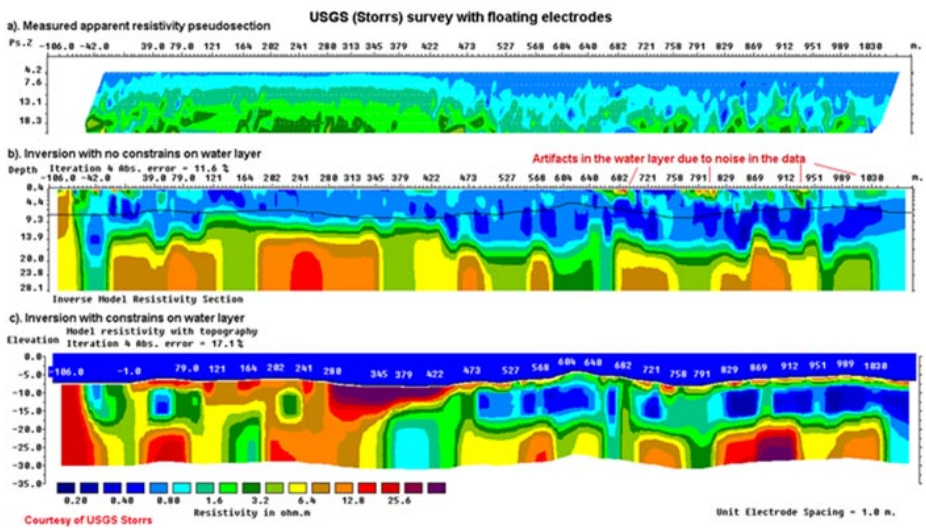

Continuous resistivity profiles along the Thames River, Norwich, Connecticut. Effective electrode spacing is 1.0 meter. Cooler colors represent regions of lower resistivity, and warmer colors regions of higher resistivity. a) (top) measured apparent resistivity pseudosection; b) (middle) inverted resistivity model with no constraints on water depth or specific conductance after four iterations with a root-mean-square error of 11.6 percent; and c) inverted resistivity model with constraints on water depth and specific conductance after four iterations with a root-mean-square error of 17.1 percent.

From Henderson et al. (2008):

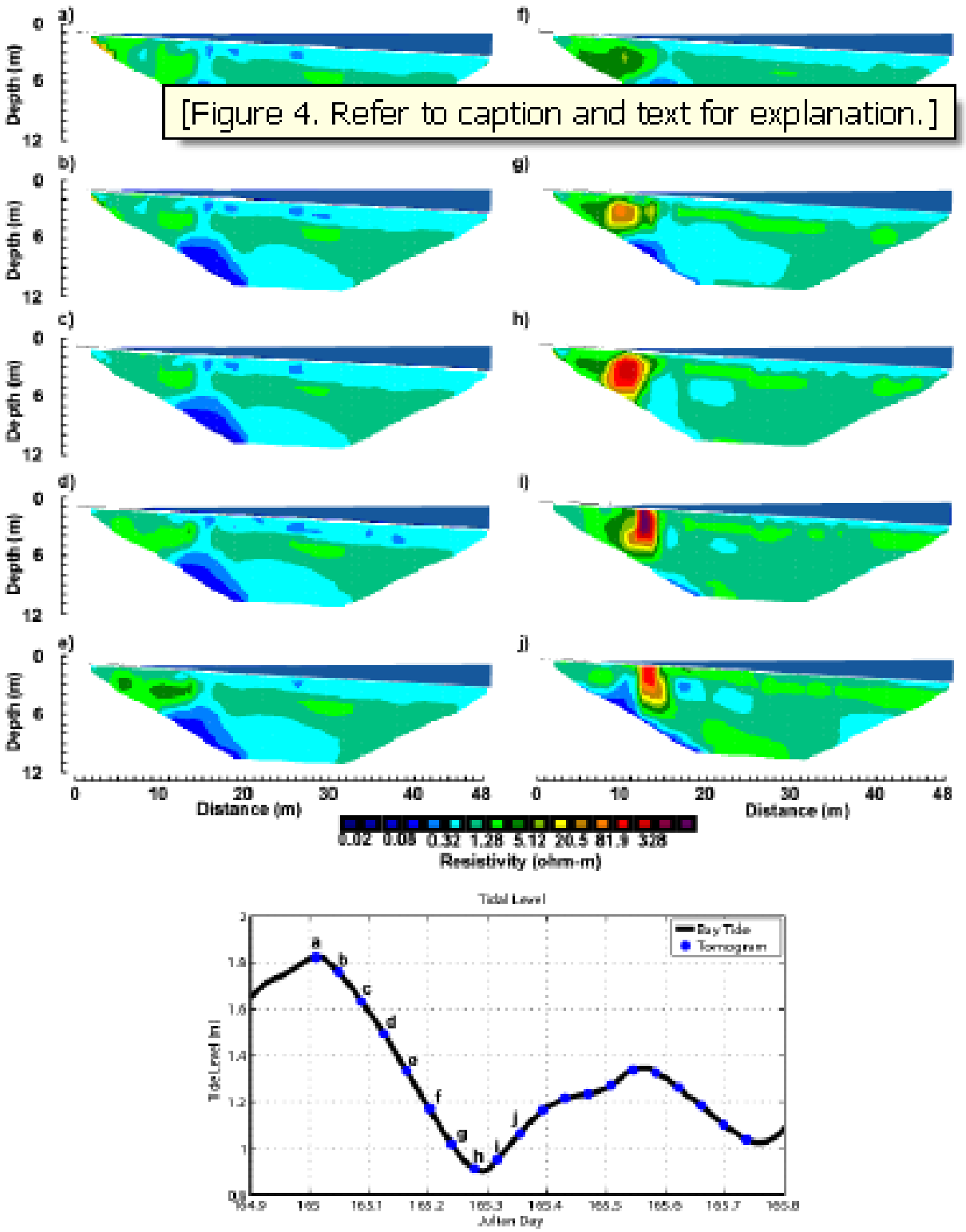

Figure 4: Tomograms for an 18-hour period (a-t). The tomograms begin at high tide (a) and progress through 1.5 tidal cycles. The tidal level corresponding to the tomograms is shown in the plots at the bottom of each page, where the blue dots are labeled with the corresponding tomogram identification letter (continued on next page).

From Crook et al. (2008):

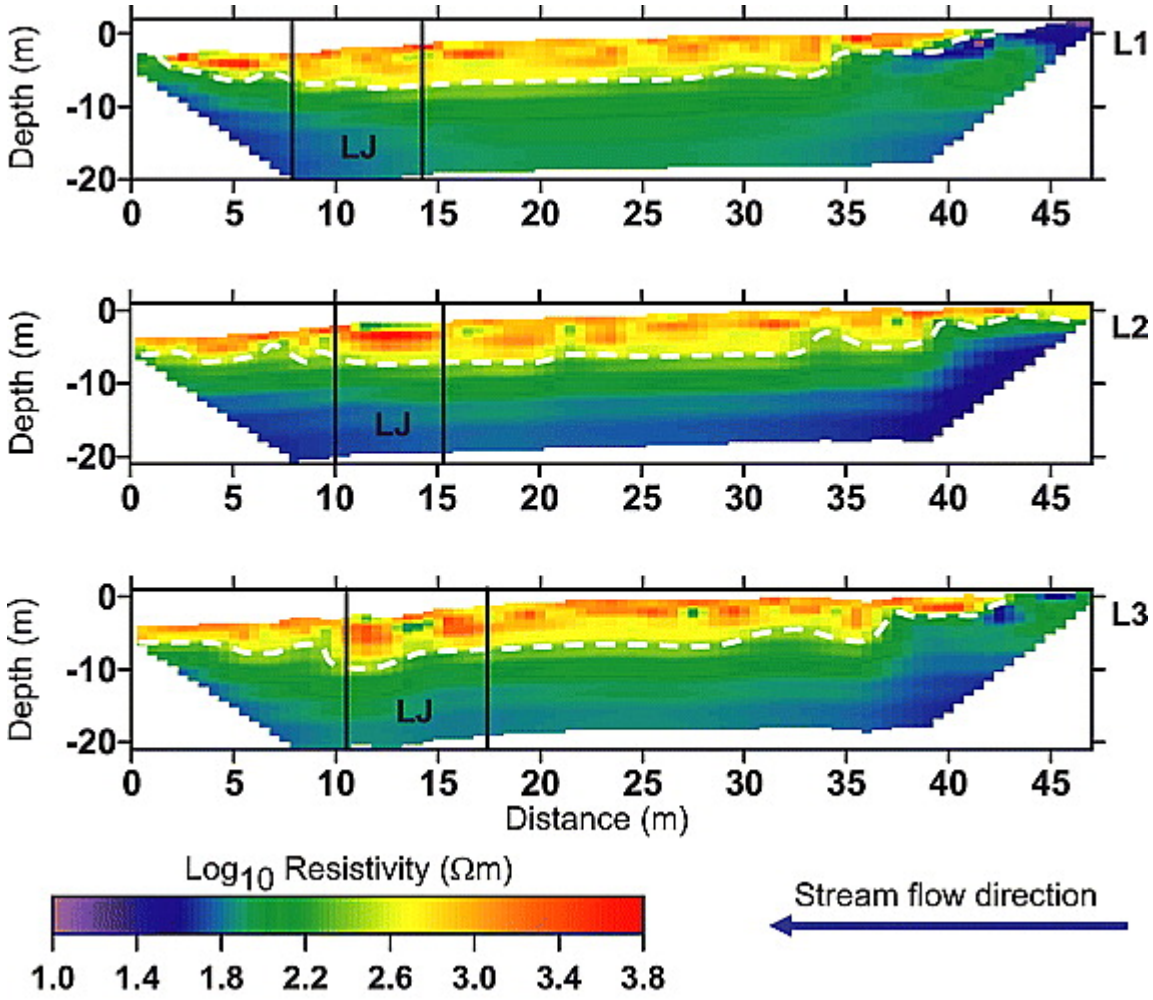

Figure 7. Electrical resistivity models for the pole-pole electrode configuration for lines L1, L2, and L3. The interval between the vertical lines, labeled LJ, indicates the surface location of the fallen logs forming the debris dam. The dashed white line indicates the interpreted bedrock-alluvial sediment boundary. Enhanced EPS [4.1 MB]

From Zarnetzke et al. (2006):

Results

Longitudinal Profiles

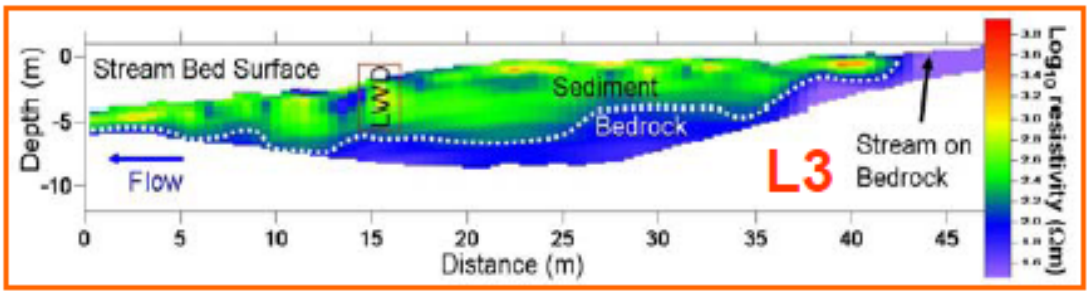

- Saturated alluvial sediment (basalt) is represented by shades of red to green, while the weathered bedrock (andesitic tuff) is blue. Mean alluvial thickness is 4.1 m with a maximum and minimum observed thickness of 8 and 0 m, respectively.

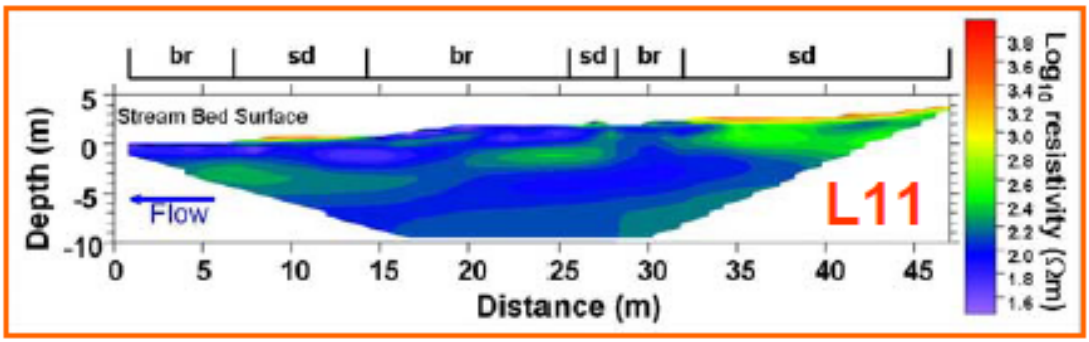

- Located immediately downstream of L3 in a historically logged reach, L11 (the groundtruth survey) illustrates strong contrast between the saturated alluvium and bedrock resistivity signatures. Along this transect the average alluvial thickness was 0.3 m.